AD NUMBER
AD491309
CLASSIFICATION CHANGES
TO: **UNCLASSIFIED**
FROM: **CONFIDENTIAL**
LIMITATION CHANGES
TO: **Approved for public release; distribution is unlimited. Document partially illegible.**
FROM: **Distribution authorized to DoD only; Test and Evaluation; MAY 1955. Other requests shall be referred to Defense Atomic Support Agency, Washington, DC. Document partially illegible.**
AUTHORITY
dasa sc-3 memo, 27 jun 1961; dna ltr, 27 mar 1980

THIS REPORT HAS BEEN DELIMITED
AND CLEARED FOR PUBLIC RELEASE
UNDER DOD DIRECTIVE 5200.20 AND
NO RESTRICTIONS ARE IMPOSED UPON
ITS USE AND DISCLOSURE.

DISTRIBUTION STATEMENT A

APPROVED FOR PUBLIC RELEASE;
DISTRIBUTION UNLIMITED.

DISCLAIMER NOTICE

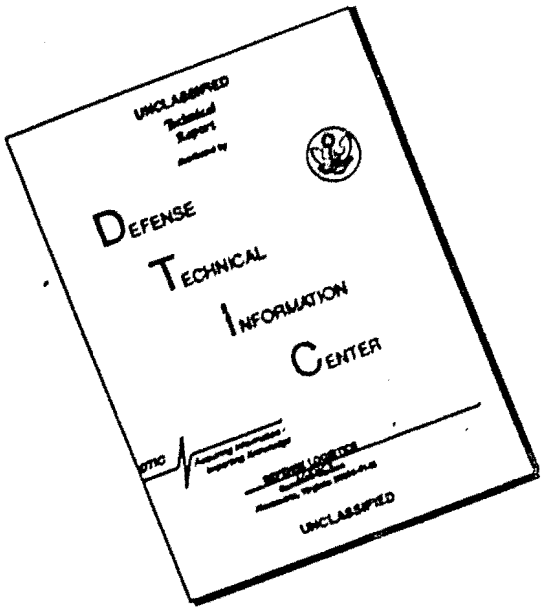

THIS DOCUMENT IS BEST QUALITY AVAILABLE. THE COPY FURNISHED TO DTIC CONTAINED A SIGNIFICANT NUMBER OF PAGES WHICH DO NOT REPRODUCE LEGIBLY.

WT-1105

This document consists of 80 pages

No. 166 of 200 copies, Series A

Operation TEAPOT

NEVADA TEST SITE

February – May 1955

Project 1.6

CRATER MEASUREMENTS

Issuance Date: July 18 1958

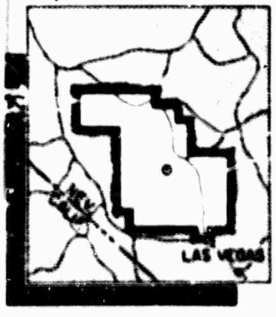

HEADQUARTERS FIELD COMMAND, ARMED FORCES SPECIAL WEAPONS PROJECT
SANDIA BASE, ALBUQUERQUE, NEW MEXICO

This document consists of 1 page
No. 166 of 200 copies, Series A

ERRATA SHEET FOR WT-1105

CRATER MEASUREMENTS

(Operation Teapot Final Report, Project 1.6)

This sheet should be inserted following Page 76 of WT-1105.

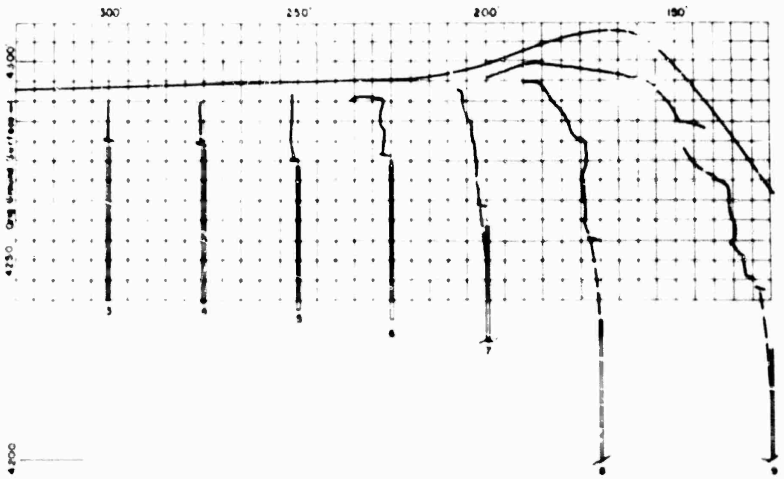

Figure A.1 Column displacement in north side of Shot 7 crater.

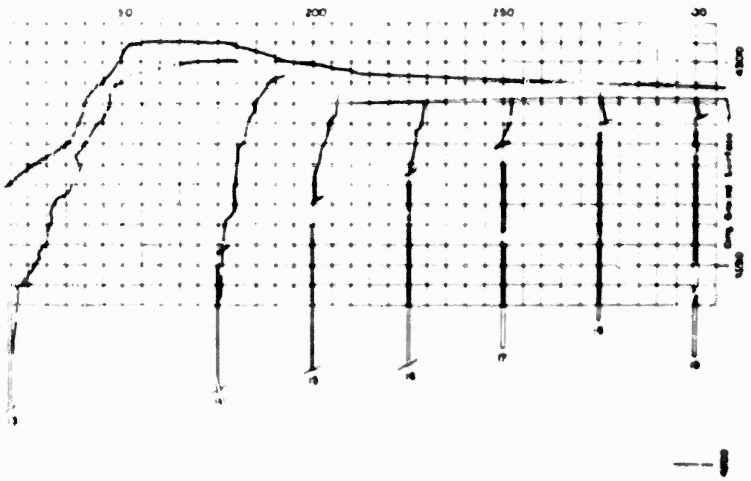

Figure A.2 Column displacement in south side of Shot 7 crater.

[redacted]

UNCLASSIFIED

WT-1105 (21) Hydrodynamic

OPERATION TEAPOT—PROJECT 1.6,

Report to the Test Director

(6) CRATER MEASUREMENTS,

(10) by John G. Lewis.

(5) ARMY Engineer Research and Development [redacted] LABS., Fort Belvoir, [redacted] VA.

[redacted]

UNCLASSIFIED

SUMMARY OF SHOT DATA, OPERATION TEAPOT

Shot	Code Name	Date	Time*	Area	Type	Latitude and Longitude of Zero Point
1	Wasp	18 February	1200	T-7-4†	762-ft Air	37° 05' 11.6536" 116° 01' 18.7366"
2	Moth	22 February	0545	T-3	500-ft Tower	37° 02' 53.3534" 116° 01' 15.4367"
3	Tesla	1 March	0530	T-9b	300-ft Tower	37° 07' 31.6737" 116° 02' 51.0077"
4	Turk	7 March	0520	T-2	500-ft Tower	37° 06' 10.4944" 116° 01' 03.1870"
5	Hornet	12 March	0520	T-3a	300-ft Tower	37° 02' 35.4943" 116° 01' 31.3874"
6	Bee	22 March	0505	T-7-1a	500-ft Tower	37° 05' 41.3360" 116° 01' 35.6474"
7	ESS	23 March	1230	T-10a	67-ft Underground	37° 10' 00.1383" 116° 03' 27.7010"
8	Apple	29 March	0455	T-4	500-ft Tower	37° 06' 42.0300" 116° 02' 09.0060"
9	Wasp'	29 March	1000	T-7-4‡	740-ft Air	37° 05' 11.6536" 116° 01' 18.7366"
10	HA	6 April	1000	T-5§	36,620-ft MSL Air	37° 01' 49.3543" 116° 00' 35.2134"
11	Post	9 April	0430	T-9c	300-ft Tower	37° 07' 10.0085" 116° 02' 03.2290"
12	MET	15 April	1115	FF	400-ft Tower	36° 47' 53.0881" 116° 00' 44.1044"
13	Apple 2	5 May	0510	T-1	500-ft Tower	36° 03' 11.3006" 116° 00' 00.0521"
14	Zucchini	15 May	0500	T-7-1a	500-ft Tower	37° 05' 41.3360" 116° 01' 35.6474"

* Approximate local time, PST prior to 24 April, PDT after 24 April.
† Actual zero point 36 feet north, 426 feet west of T-7-4.
‡ Actual zero point 54 feet north, 62 feet west of T-7-4.
§ Actual zero point 36 feet south, 397 feet west of T-5.

ABSTRACT

Vertical shafts of colored sand were placed along one diameter through ground zero on Shot 7 to give a permanent record of the true crater. Measurement of the physical characteristics of the apparent crater and lip, and the true crater were made.

The nuclear data obtained from Operation JANGLE surface and underground shots and TEAPOT Shot 7 were correlated with previous high explosive (HE) test results. Scaled curves of dimensions versus depth of burial with correlation between HE and nuclear bursts were developed for the Nevada Test Site soil as well as for several other soil types for which reliable HE data are available.

Particular attention was given to the definition of the terms apparent and true craters, in light of their meaning being based on the movement of the soil, as depicted by the colored sand columns. A brief examination is made of the effects of energy density on the TNT equivalence of underground nuclear bursts. The charge emplacement configuration can play a significant role in determining the TNT equivalence of a particular burst.

FOREWORD

This report presents the final results of one of the 56 projects comprising the Military Effects Program of Operation Teapot, which included 14 test detonations at the Nevada Test Site in 1955.

For overall Teapot military-effects information, the reader is referred to "Summary Report of the Technical Director, Military Effects Program," WT-1153, which includes the following: (1) a description of each detonation including yield, zero-point environment, type of device, ambient atmospheric conditions, etc.; (2) a discussion of project results; (3) a summary of the objectives and results of each project; and (4) a listing of project reports for the Military Effects Program.

PREFACE

The original ideas for the use of colored sand columns for measurement of cratering effects were conceived by Beauregard Perkins, Jr., Ballistics Research Laboratories. The author is greatly indebted to Mr. Perkins for his consultation and assistance during the planning and operational phases of both the HE and nuclear portions of the test and in the interpretation of the data obtained.

The assistance of the following people is gratefully acknowledged by the author: (1) CDR. W. M. McLellan, Lt. Col. J. G. James, Major H. T. Bingham, LCDR. Fred Clark of Programs Section; Lt. Col. J. J. Haley and staff, Requirements Section; and the staff of the Directorate of Weapons Effects Tests, Field Command, AFSWP; (2) Captain R. LaPointe and Captain W. Saye and staffs of the Nevada Test Site Detachment; (3) the personnel of the Stanford Research Institute field group, under L. M. Swift; (4) Lt. Col. John Pickering, LCDR. W. J. Christiansen, and Lt. B. S. Merrill, Blast Branch, AFSWP; (5) Pvts. L. C. Essig and William Murphy of the Ballistics Research Laboratory; and (6) Colonel E. F. Klinke, Major R. A. Bertram, Dr. T. G. Walsh, Captain R. C. Mason, F. A. Pieper, Owen Richmond, J. W. Holbrook, Lt. B. A. Homer, Pvts. N. P. Jokerst, Warren Hils, and J. E. Taylor, and Pfc. Lionel Stein, all of the Engineer Research and Development Laboratories.

CONTENTS

FIGURES

Chapter I
INTRODUCTION

1.1 OBJECTIVE

The objective of this project was to determine the physical characteristics of the crater and lip formed by the underground explosion of a nuclear device. These crater characteristics are utilized in establishing empirical scaling curves for the cratering effects from underground bursts. The curves apply to soil conditions found at the Nevada Test Site (NTS) and were obtained by interpolation between JANGLE surface shot (S), JANGLE underground shot (U), TEAPOT Shot 7, and extrapolation from high explosives (HE). In addition, an effort is made to construct nuclear cratering curves for other soil types for which reliable and applicable HE data are available.

Correlation between nuclear weapons and HE cratering phenomena is desired for various scale depths of burial for the particular soil conditions at NTS. One of the important factors in interpreting the results of a crater measurement test is the problem of definition of the various crater characteristics. Therefore, a further objective of this project was to define such variables as apparent crater and true crater for the Nevada soil, in order to make the results of the nuclear experiment more easily interpreted.

1.2 BACKGROUND

Two nuclear devices of 1.2-kt yield, one a near surface burst (3.5 feet above the surface) and the other an underground burst (17 feet depth of burial), were detonated at JANGLE in 1951. Only measurements of the apparent craters were obtained at this test because no provision had been made for permanent instrumentation to allow the measurement of the true crater after decay of the residual activity. After a time lapse, sufficient to reduce the radiation hazard, accurate measurement of the true crater dimensions was impossible, since during the waiting period the area was exposed to the elements which caused the surface soil to be blown about by the wind and consolidated by rain and snow. (Reference 1).

A distinction between the meaning of the terms apparent crater and true crater as intended in this report is warranted. In Figure 1.1, a typical crater formed by the detonation of an explosive underground is shown. The line labeled apparent crater denotes the crater which remains after all ejected material has fallen back to earth.

The true crater is defined as the volume bounded by that surface which generally lies at some greater depth than the apparent crater, and which represents the limiting distance from the explosion at which the material originally composing the crater was completely disassociated from the underlying material.

The true crater dimension is the one which should receive the closest attention with regard to scaling of effects and partition of energy --- the apparent crater is too easily affected by such factors

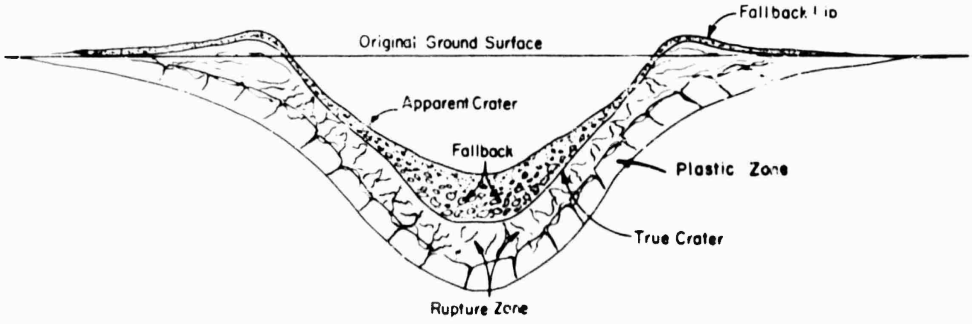

Figure 1.1 Profile of craters from an underground explosion.

as surface wind conditions and angle of repose of the distrubed soil. In addition, the rupture zones are too difficult to measure in most soil types. Rupture zones are quite easily measured in high-clay-content soils, but are almost impossible to define in sandy soils.

In order to give more confidence to the experimental technique used in Project 1.6 for determining the true crater measurements and also to define this true crater in NTS soil, an HE test was conducted at NTS during the fall of 1954. The results of this test are given in Chapter 2.

Chapter 2
PRETEST HIGH EXPLOSIVES PROGRAM

2.1 THEORY

The field of underground explosion effects has had to be approched from the empirical point of view in order to achieve any semblance of understanding. The factor contributing most to this situation is the earth itself, which by the very nature of its extreme non-homogeneity makes mathematical models and equations of state difficult to establish. The lack of suitable ground-shock instrumentation has retarded the determination of paramenters influencing the phenomena; this in turn has retarded the development of a suitable theory.

The earth lends itself to one form of measurement, cratering, which air and water do not, that has been valuable for study. When the earth is ruptured by an explosion, a record of rearranged, pulverised, sheared, and even fuzed earth is left behind which can be empirically studied while the development of transient effects measurements is advancing. Measurements have been made of the apparent crater, that crater existing after all fallback, as the basis for criteria of damage. The variables of the apparent crater are: diameter at original ground level, depth, lip diameter, lip height, and volume. In some instances, attempts have also been made to measure the true crater dimensions either by probing with rods or by excavating a vertical cross section to find undisturbed material. The Ballistic Research Laboratories (BRL) has experimented successfully in sand and clay using vertical columns of colored sand to give permanent records of displacements and shear. These results were from very small HE charges and are reported in Reference 2.

The BRL technique showed great promise as a means of obtaining a vertical cross section of a crater below and beyond the apparent crater, and in giving indications of the extent of the material movement in the regions ranging from complete shear and ejection to no shear and minor displacement. It also indicated the mechanism of lip formation, giving impetus to forming a tangible definition of the true crater and to extrapolating such a definition to the nuclear case and other soil types as a means of understanding the partition of energy of undergound explosions. The true crater appears to be a more logical parameter for energy determination, principally because it is not affected as much as the apparent crater by the post-explosion phenomena of fallback, fallout, angle of repose of the disturbed earth, and meteorological conditions.

The term energy partition is discussed briefly here to avoid confusion in terminology. When a high-energy source is suddenly formed

by the detonation of a charge, a volume approximately the size of the charge and containing this total energy can be said to exist for an instant after detonation. The amount of energy released per unit weight of explosive is the energy density of the explosive. The term energy density is often used to describe high explosives according to their brisance or shattering power as distinguished from their total work capability. Brisance in high explosives is dependent upon the suddenness with which the gaseous products of an explosion are liberated, and the rate of detonation is at least a major factor in determining brisance. A new definition of energy density is required when describing the thermodynamic and hydrodynamic states of a nuclear explosion from its time of detonation until the transfer of its energy to the surrounding medium becomes faster by shock than by radiation --- the end of radiative transport. This is energy density in terms of energy per unit volume. Throughout the remainder of this report this latter definition of energy density will be used unless stated otherwise.

Since the gasball of a high explosive charge is obtained by chemical decomposition, its energy density is determined by the volume of the undetonated charge. However, a nuclear explosion must create its gasball from the weapon fragments and the surrounding medium. This process, known as radiative transport, is estimated to end when the isothermal sphere has cooled to a temperature of about 300,000 degrees Kelvin. It follows that the volume of the gasball at this temperature will be dependent upon the medium in which the detonation occurs (Reference 7). The amount and rate of work done on surrounding medium by the energy of an explosion is seriously affected by the energy density of that explosion. The energy density factor alone can lead to some of the difficulties of correlating atomic and HE explosions, since their respective initial energy densities can differ greatly, possibly by a factor of 10^7. For nuclear airbursts, this large energy-density difference manifests itself by loss of a large percentage of total energy through radiation, whereas the relatively low-temperature HE burst loses only a small percentage in this manner.

A nuclear airburst is usually referred to as having a mechanical, or blast, efficiency of 40 to 50 percent relative to TNT (sometimes better expressed as a TNT equivalent of 40 to 50 percent in mechanical energy). This mechanical efficiency is somewhat harder to define for explosions which travel through an interface, such as from ground to air; but again, the mechanical effects of the TNT explosion can be considered as 100 percent, and the nuclear effects can be evaluated to give a TNT equivalent.

It is reasonable to assume that the mechanical energy will increase when the surrounding medium is highly opaque to thermal emission, as in underground nuclear bursts, rather than when it is relatively transparent, as in airbursts. In either case, however, the TNT equivalent does not account for the total energy release. To present the partition of mechanical energy from an underground burst as the depth of burial is greatly increased, the energy appearing in the form of the crater, ground shock, and air shock could be

plotted as is shown in Figure 2.1. A most important point about this comparison is that the apparent crater does not turn out to be a good effects measurement, with respect to energy partition, as the depth is increased; conversely, the true crater continues to indicate work done on the ground, even to extreme depths. There are zones beyond the true-crater which would be better for measurement of work done; however, these must be measurable in all types of soil to be useful --- unfortunately, this is not the case. These zones beyond the true crater are usually referred to as rupture zones. In order to measure the maximum work done on the soil, it may be reasoned that the extremes of this rupture zone are more indicative of total work than are the limits of the true crater. In a few soil types, such as sand or the NTS soil, these rupture zones cannot be measured easily, if at all.

The next step was carried out by the United States Army Engineer Research and Development Laboratories (USAERDL), to see if the new technique worked well for charges larger than those used at BRL, and it was found to provide excellent results with charges in the 200-pound category. The problem then arose as to the selection of the proper column material, color, and configuration for the **TEAPOT** crater-measurement project, since this would be a one-shot participation, with no chance for subsequent modifications of techniques. It was decided that USAERDL would instrument the final phase of the Stanford Research Institute (SRI) Mole project at the JANGLE U - TEAPOT Shot 7 site and determine significant soil factors prior to Shot 7. Further, information was desired as to whether the apparent crater at JANGLE U was also a true crater, and whether it would give a direct comparison between the colored-sand-column and the probing technique of true-crater measurement.

The objective was to establish a definition of a true crater using sand columns --- not to validate other measurements, particularly in Nevada soil --- in order to give more understanding and reliability to the Shot 7 results and correlation with the high explosive tests in other soil types. These will ultimately follow in searching for more exact solutions to the problems of employment and effects of underground explosions.

In addition to these current and long range problems, it was important to predict the effects for Shot 7, in order to properly plan the location of test structures, basic instrumentation, and columns for Project 1.6.

2.2 PROCEDURE

During the period 18 October through 4 November 1954, the SRI detonated six 256-pound spherical TNT charges at the JANGLE U site. Four of these, at scaled depths of 0.26, 0.50, 0.75, and 1.0 ft/lb$^{1/3}$, were instrumented for taking true crater measurements using nine vertical columns along one diameter through ground zero (including one column directly below the charge). The holes for these columns were drilled with a 6-inch-diameter auger, ranging in depth from 4

feet for the outer columns to 18 feet for the inner ones. The column configurations for Shots 401, 402, and 405 are shown in Figure 2.2, and the configuration for Shot 404 is shown in Figure 2.3. The column depths were extended for Shot 404 because of the greater scaled depth of burial of the charge.

Two types of fill material were used in the columns: asphalt and colored sand. The strength of the asphalt columns was varied, as was the amount of water or liquid content of the sand columns.

After each shot had been fired apparent crater measurements were made. After plotting this profile, one half of the crater was

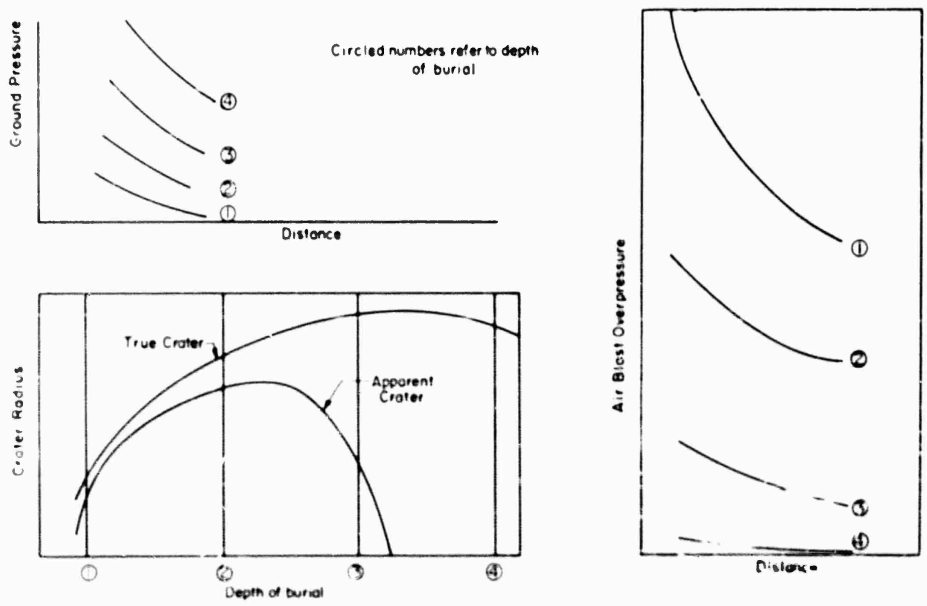

Figure 2.1 Schematic plan of the partition of blast energy from an underground explosion between effects above and below ground.

excavated away from the columns using a drag line to considerably enlarge half of the crater, taking care not to disturb their position. After excavation by drag line, hand tools were used to uncover the columns one at a time. As portions of the columns were uncovered, they were surveyed, photographed and plotted on a profile as shown in Figures 2.4 to 2.7. It was originally planned to space the center columns at 2-feet intervals but this proved unsatisfactory for

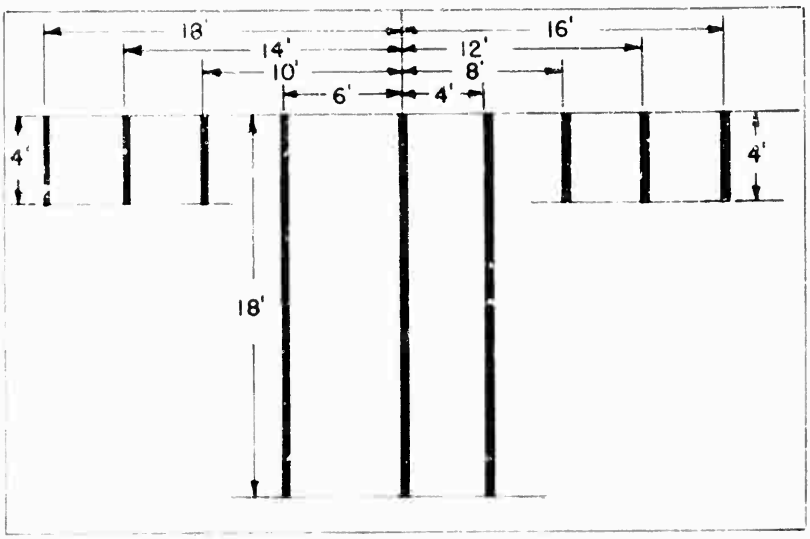

Figure 2.2 Preshot column configurations for Shots 401, 402 and 405.

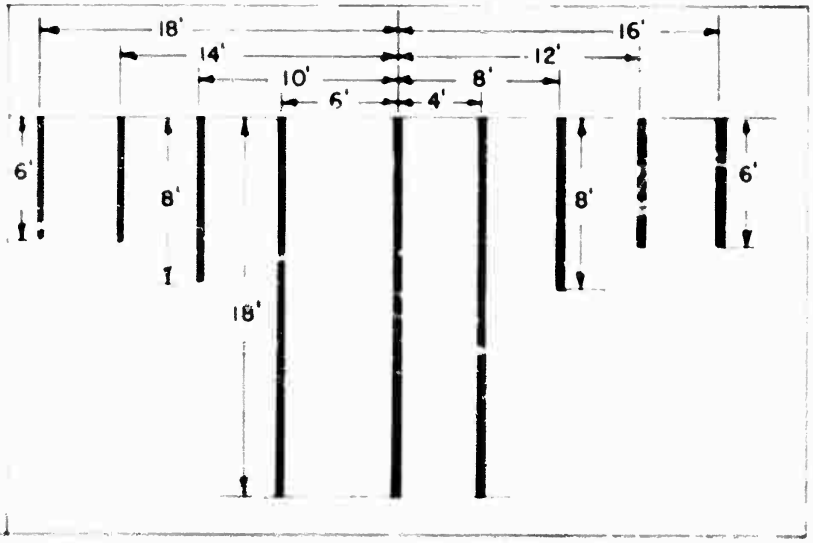

Figure 2.3 Preshot column configurations for Shot 404.

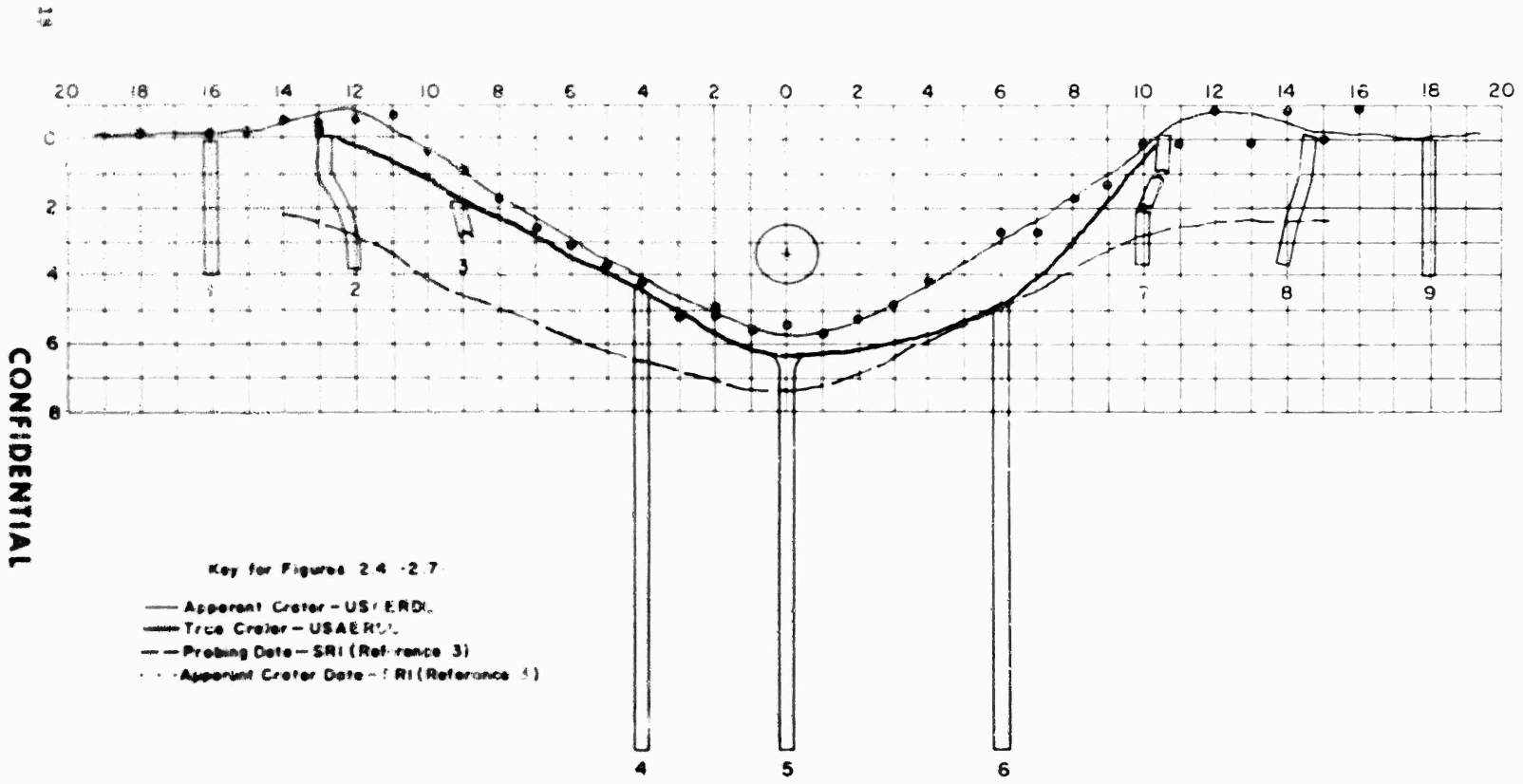

Figure 2.4 Shot 401, $\lambda_c = 0.5$. Columns 1-4, sand; columns 5-9.

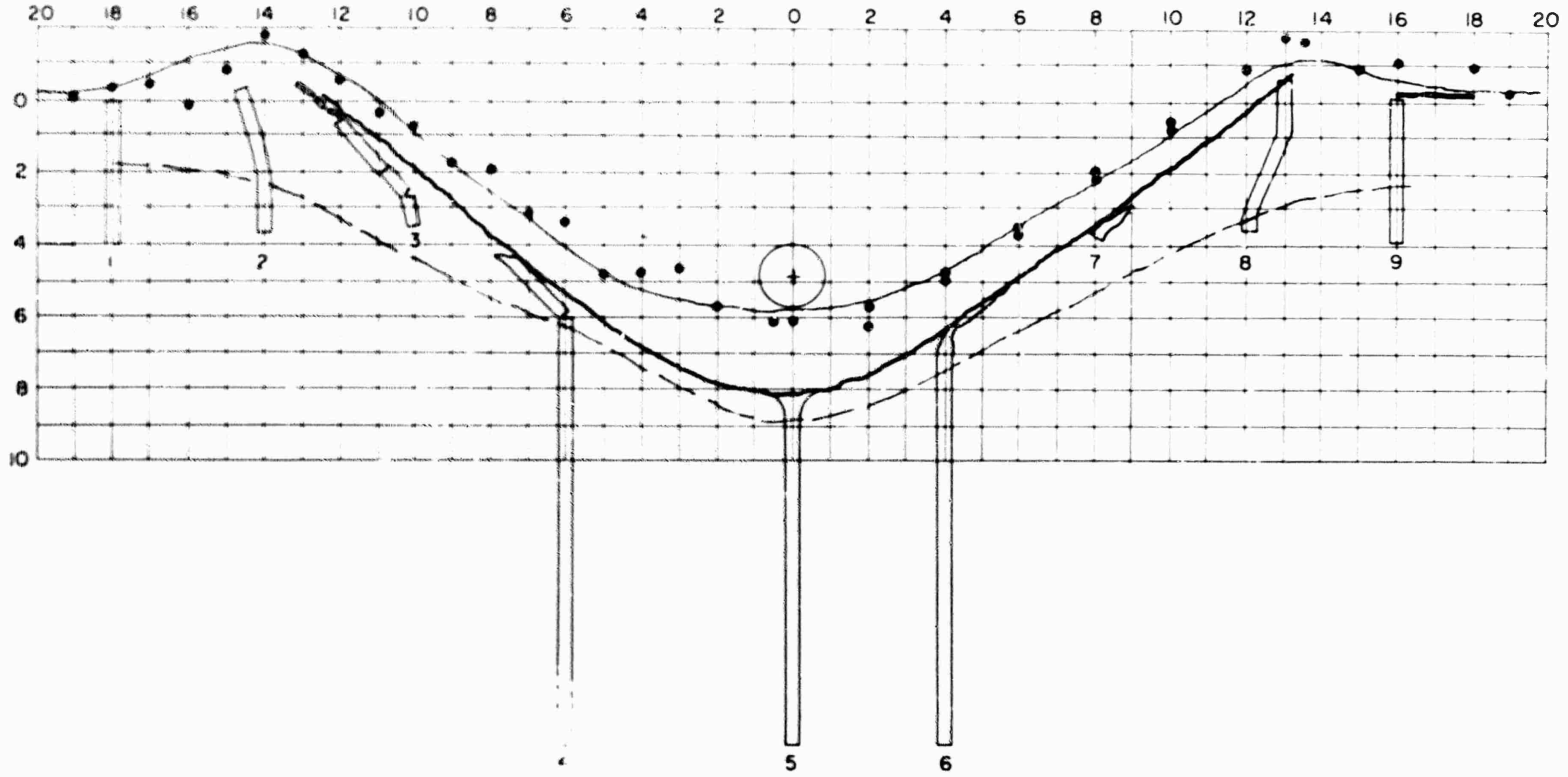

Figure 2.5 Shot 402, $\lambda_c = 0.75$. All columns sand.

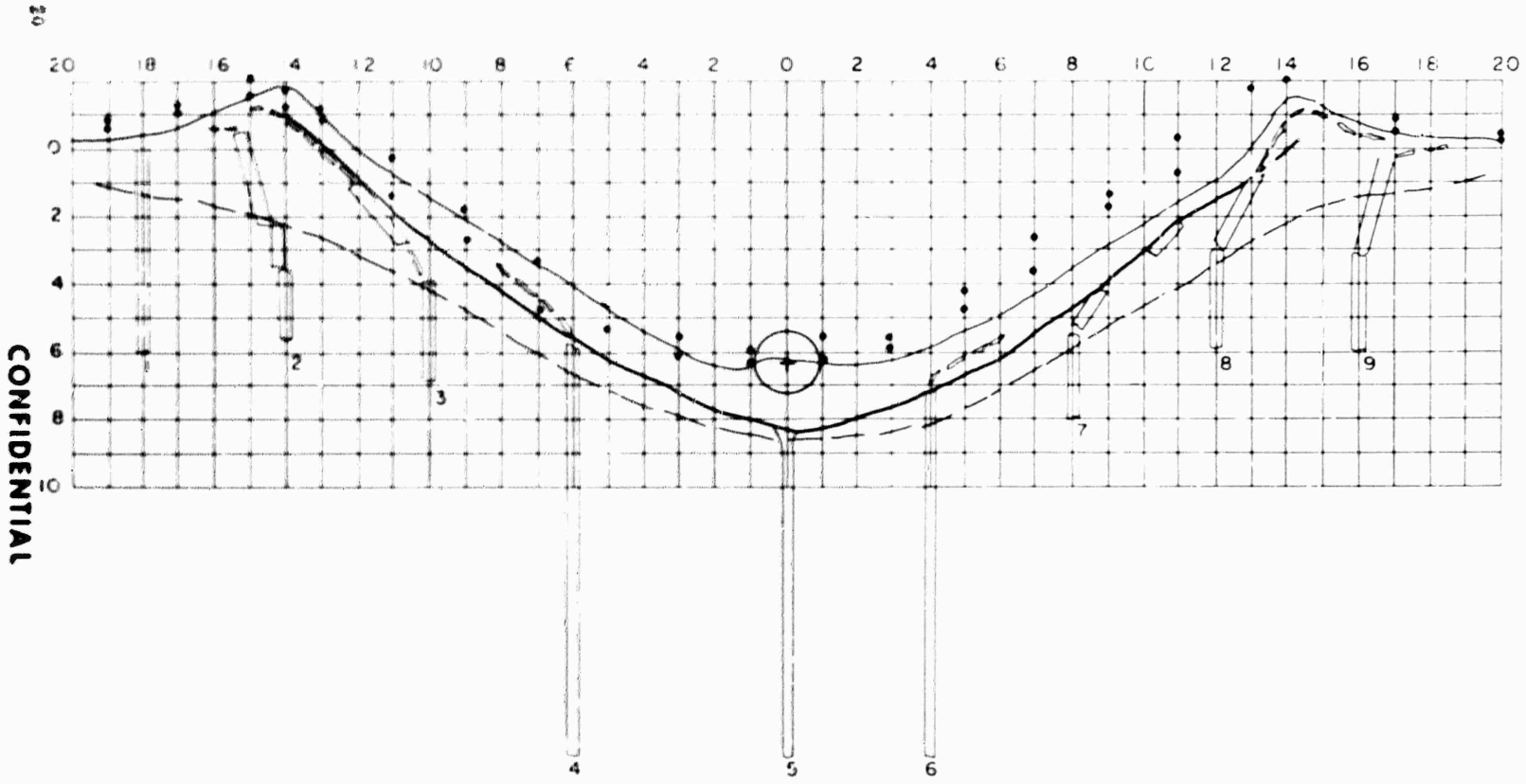

Figure 2.6 Shot 404, $\lambda_c = 1.0$. Columns 1-5, asphalt; columns 6-9, sand.

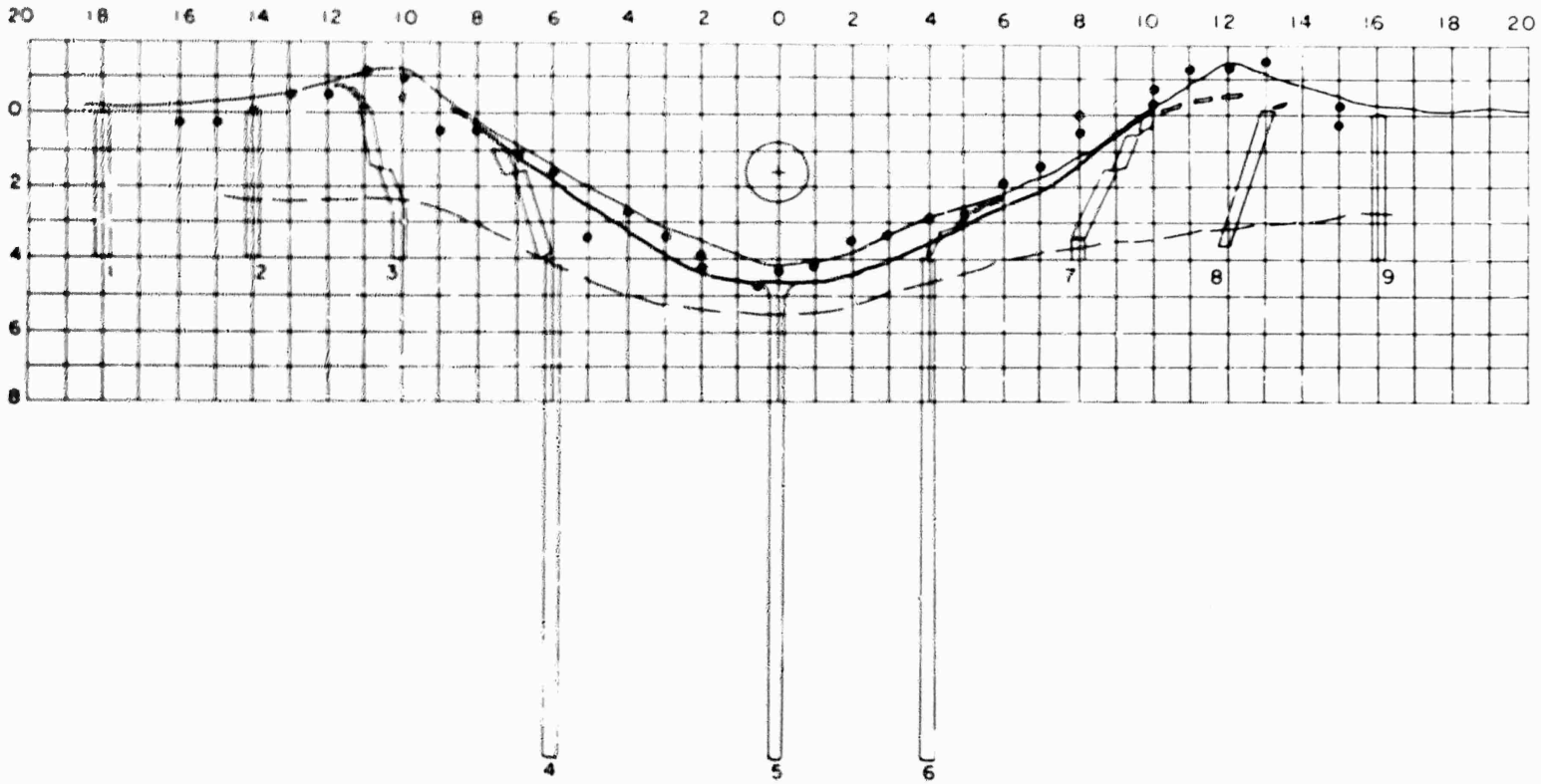

Figure 2.7 Shot 405, $\lambda_c = 0.26$. Columns 1-5, sand; columns 6-9, asphalt.

drilling the holes without interaction. Thus a plan having spacing no closer than 4-feet was adopted and worked well.

2.3 RESULTS

The results of Shots 401, 402, 404, and 405 were quite satisfactory in establishing the true crater and in developing the additional operational technique needed for the efficient conduct of Project 1.6. The profiles shown in Figures 2.4 to 2.7 give the results obtained by probing as well as the USAERDL column data. These SRI data are taken from Reference 3 and vary somewhat from the USAERDL apparent-crater profile obtained in a similar manner but along a different diameter: that of the colored columns. For comparisons with previous data, the SRI measurements will be used for the apparent-crater and the USAERDL measurements for the true-crater.

2.3.1 Shot 401. This shot was at a scaled depth of $z = 0.5$ and was instrumented with asphalt columns to one side of ground zero and below the charge, and the red-sand columns on the other side of ground zero. The column positions are shown in Figure 2.2. The three outer columns on each side were approximately 2.5 inches in diameter. These smaller-diameter columns were made by standing a steel cylinder in the center of the 6-inch-diameter hole and alternately adding fill material around the outside, colored material to the inside, and pulling the steel cylinder from the hole to the surface of the ground. This technique was quite satisfactory; however, it was unnecessary for the sand columns because the colored fill is of the same soil that was drilled from the hole and strength was unaffected by adding the water-base paint coloring to the 6-inch-diameter hole.

Columns 1 and 9 showed no displacement from the explosion. Columns 2 and 8 (shown in Figures 2.8 and 2.10 respectively) were apparently in the rupture zone of the crater and just beyond the true crater. Column 7 (Figure 2.9) was not symmetrical with Column 2 and presented a difficulty in selecting the base of the true crater at this point due to the lack of columns sufficiently close on each side. Column 3 was severely ruptured and ejected, with only a small section at the bottom being recovered. This bottom piece was displaced both radially and vertically. Columns 4 and 6 were cleanly sheared off (Figure 2.11) together with Column 5, which was mushroomed by the blast, as were all the center columns of the subsequent shots. The tops of these columns represented the base of the true crater profile. The dip in the true crater profile at Column 6 was undoubtedly caused by belling of the hole during drilling, which disturbed this zone and reduced its shear strength. An average cross section obtained by SRI using the probing technique is also shown on Figure 2.4. It falls well below the true crater and into what might be called the limit of the extreme rupture zone.

2.3.2 Shot 402. The crater from Shot 402 was more symmetrical than for 401 (Figure 2.5). This shot was at a scaled depth of

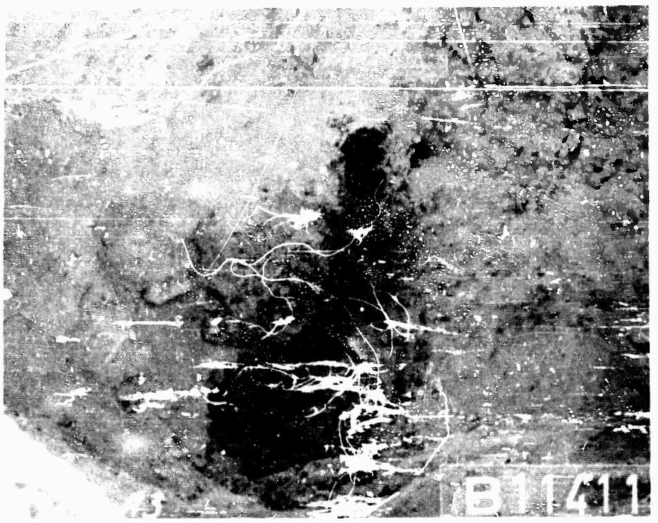

Figure 2.9 Column 7 of shot 401, 2.5 inch diameter, 10 feet from ground zero, asphalt column.

Figure 2.3 Column 2 of shot 401, 2.5-inch diameter, 12 feet from ground zero, filled with orange-colored sand.

Figure 2.10 Column 8 of shot 401, 2.5-inch diameter, 14 feet from ground zero, asphalt column.

Figure 2.11 From left to right: Columns 4,5 and 6 of shot 401. Column 4, orange colored sand, 6-inch diameter, 4 feet from ground zero; Columns 5 and 6 asphalt, 6-inches diameter, at ground zero and 6-feet from ground zero, respectively.

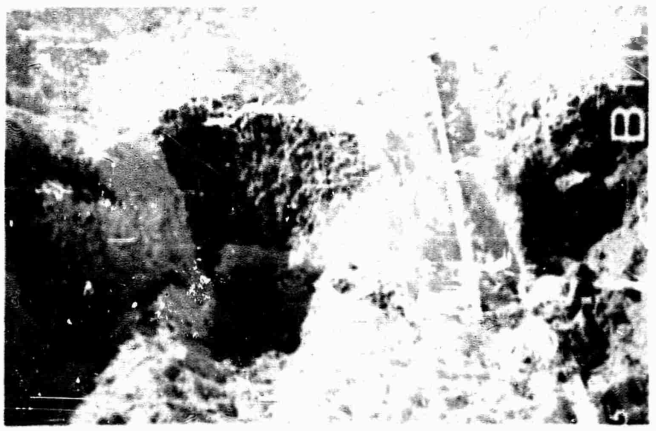

λ_c = 0.75 and was instrumented with sand columns only in alternate colors of yellow and white. The white was a poor selection, since it gave very little contract to the soil itself. Again, the SRI probe data fell below the USAERDL true crater line, especially at the greater distances from ground zero. The sand columns here began to show a superiority over the asphalt for producing better records and also for giving a column strength more nearly equal to that of the surrounding medium, thereby indicating a more reliable measurement. On this shot, a phenomenon was noticed at the top of Column 9 (an exposed view of this column is shown in Figure 2.12). The column was sheared in a horizontal plane by the action of the lip formation. This left a thin line of colored sand, shown in diagram in Figure 2.12 and by the thin, white trace in line with the trowel shown in Figure 2.12. This phenomenon was first noticed in previous work (Reference 2) and verified the idea that the lip is formed principally by horizontal radial displacement of closer-in material sliding over the original ground surface. There is also evidence of vertical displacement in the formation of the lip as will be seen in examination of the TEAPOT Shot 7 results. This vertical motion is caused by compression in the rupture and plastic zones which causes the soil nearest the surface to move in the direction of least resistance which in this instance is upward. A paste-like sand having the consistency of a thick quicksand, which is shown in Figure 2.13, was used in Column 3 but proved unsatisfactory because its added strength caused bending rather than a shearing movement.

2.3.3 Shot 404. This shot was at a scaled depth of λ_c = 1.0, and the results were very similar to those for Shot 402, the crater having a slightly larger volume. The trace material in the lip was again observed, and, in this instance from two columns on each side, gave a clearer indication of this formation. Asphalt was used again on this shot in Columns 1 to 4; but when it was mixed thin enough to form a suitable column, the asphalt was nothing more than a thin coloring material which could be better done by the water-base paint. Figure 2.14 shows a major portion of Column 2, which was outside the true crater zone, but it shows two well-defined shear planes within the zone of rupture as well as a thin shearing trace at the top of the column similar to that indicated in Shot 402. All the columns for this shot were a full 6 inches in diameter with Columns 1, 2, 6 and 9 being extended to 6 feet, and Columns 3 and 7 being extended to 8 feet to handle the greater depth of burial.

2.3.4 Shot 405. This shot was interesting because it was at a depth (λ_c = 0.26) nearer the JANGLE U scaled depth (λ_c = 0.14) and gave an indication that there may be a trend toward less difference between the true and apparent craters as the scaled depth is decreased. Colored sand was used in Columns 1 to 5, and an asphalt-colored sand, identical with that used in Shot 404, was used in the remaining columns. Figure 2.15 shows a broad view of the left half of the crater comprising Columns 4 to 8. These two figures used together with Figure 2.7 clearly show the true crater zone. Column 3, shown in Figure 2.17, was entirely outside the true crater and in the zone of

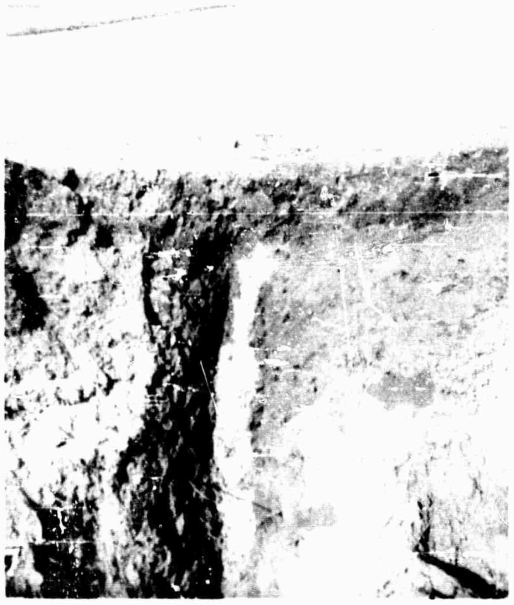

Figure 2.12 Column 9 of Shot 402, 2.5-in diameter, white-colored sand, 16 feet from ground zero

Figure 2.13 Column 3 of Shot 402, 2.5-in diameter, white sand column with a high water content, located 10 feet from ground zero

Figure 2.14 Column 2 of Shot 404, 2.5-in diameter, white-colored sand column, located 14 feet ground zero.

Figure 2.15 Column 2 through 5 of Shot 405.

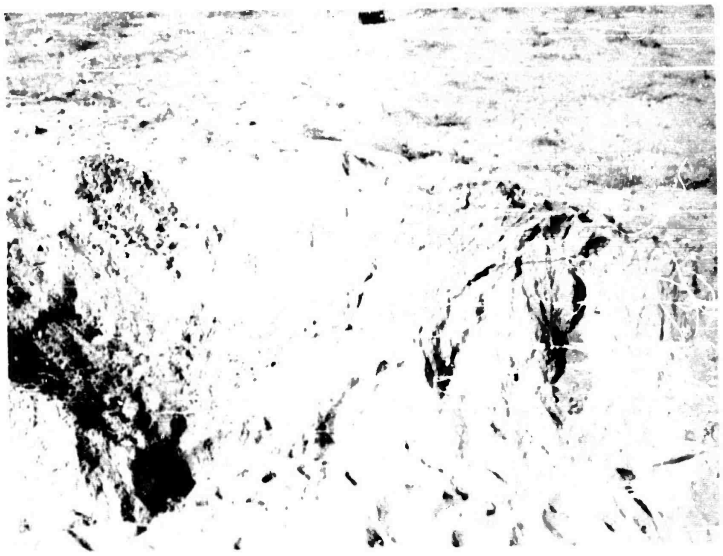

Figure 2.16 Columns 5 through 8 of shot 405.

Figure 2.17 Column 3 of Shot 405, 2.5-in diameter, yellow-colored sand column, located 10 feet from ground zero.

Figure 2.18 Column 6 of Shot 405, 6-in diameter, asphalt-colored sand column, located 4 feet from ground zero.

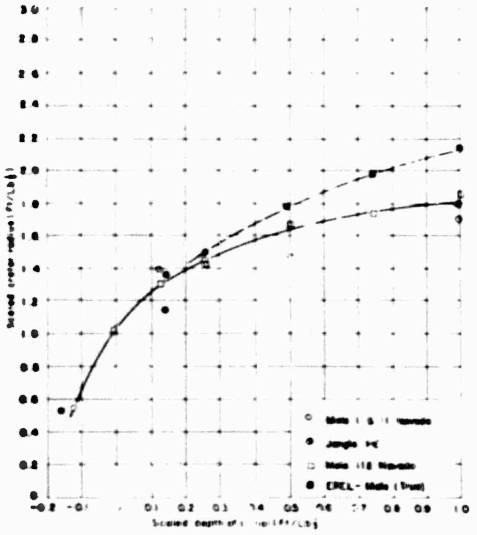

Figure 2.19 Scaled crater radius versus scaled depth of burial.

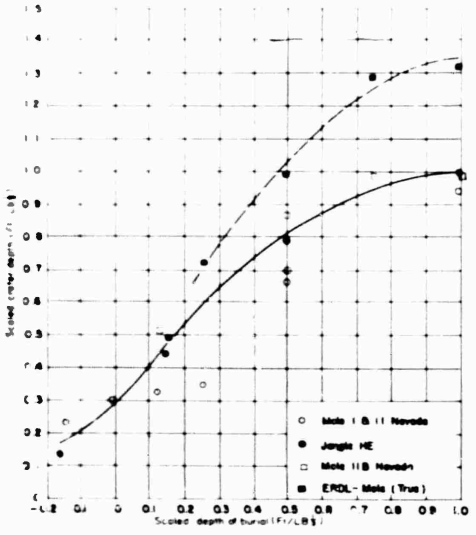

Figure 2.20 Scaled crater depth versus scaled depth of burial.

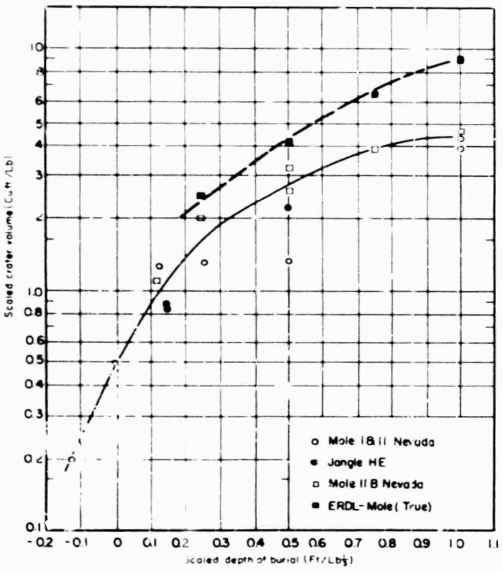

Figure 2.21 Scaled crater volume versus scaled depth of burial.

TABLE 2.1 - ERDL-MOLE CRATER DATA

Charge Number	Charge Weight (lb)	Scaled Depth ($ft/lb^{1/3}$)	Apparent Crater						True Crater					
			Radius*		Depth*		Volume		Radius		Depth		Volume	
			(ft)	($ft/lb^{1/3}$)	(ft)	($ft/lb^{1/3}$)	(ft^3)	(ft^3/lb)	(ft)	($ft/lb^{1/3}$)	(ft)	($ft/lb^{1/3}$)	(ft^3)	(ft^3/lb)
401	256	0.5	10.58	1.67	5.5	0.87	850	3.3	11.3	1.78	6.3	0.99	1182	4.6
402	256	0.75	11.10	1.75	6.2	0.98	980	3.8	12.5	1.97	8.2	1.29	1687	6.6
403	256	0.13	8.33	1.31	3.35	0.53	310	1.2	---	---	---	---	---	---
404	256	1.0	11.78	1.86	6.25	0.98	1200	4.7	14.2	2.23	8.4	1.32	2358	9.2
405	256	0.36	9.18	1.45	4.6	0.72	525	2.0	9.3	1.46	4.6	0.72	626	2.4
406	256	0.50	10.0	1.58	4.45	0.70	700	2.7	---	---	---	---	---	---

* Reference 3

TABLE 2.2 - HE CRATER DATA OBTAINED IN THE NTS SOIL

Charge Number	Charge Weight (lb)	Scaled Depth ($ft/lb^{1/3}$)	Apparent Radius		Apparent Depth		Apparent Volume	
			(ft)	($ft/lb^{1/3}$)	(ft)	($ft/lb^{1/3}$)	(ft^3)	(ft^3/lb)
HE-1	2,560	0.15	18.4	1.34	6.8	0.49	2,200	0.86
HE-2	40 000	0.15	38.0	1.11	15.0	0.44	35,000	0.87
HE-3	2,560	0.5	20.0	1.46	10.8	0.79	6,000	2.35
HE-4	2,560	- 0.15	7.0	0.51	1.9	0.14	123	0.05
202	256	1.0	11.5	1.81	6.0	0.95	1,000	3.9
203	256	0.5	8.4	1.32	4.2	0.66	360	1.4
204	256	0.25	9.2	1.45	2.2	0.35	365	1.4
205	256	0.13	8.8	1.38	2.1	0.33	325	1.3
206	256	0.00	6.4	1.01	1.9	0.30	135	0.5
207	256	- 0.13	3.5	0.55	1.5	0.24	46	0.2
212	256	1.0	10.7	1.67	6.35	1.00	1,140	4.5

rupture, having several small shear planes. Figure 2.18 clearly shows a major shear plane, again located in the rupture zone and possibly associated with a stratified layer in the subsurface.

2.4 DISCUSSION

The HE shot data cannot be used as absolute values for scaling of true crater data for Nevada soil, because there were only four shots and one charge size. However, from the plot of the apparent-crater data from these shots, as compared with those from previous MOLE data and the JANGLE HE data (see Tables 2.1 and 2.2) it is apparent that all the charges detonated fully and that the points for scaled crater radius fall on the curve based on previous data. This plot is given in Figure 2.19. The USAERDL true-crater data, as given in Table 2.1 and plotted above this same curve, do not appear unrealistic. They show a trend to less difference between apparent and true craters as the scaled depth of burial is decreased. Figures 2.20 and 2.21 show plots of scaled crater depth and volume versus scaled depth of burial from the data in Tables 2.1 and 2.2.

The data, as shown in the plates and profile plots, might give a misleading impression with regard to what is meant by the shear of some of the columns at various places below the indicated true-crater lines. It is not felt that this shear, characterized by relatively small displacement (see Figures 2.9, 2.14, and 2.17), is a valid crater measurement, rather it is associated with low soil strength or stratification weaknesses. Thus, it gives a measurement with meaning only to the shot configuration and soil condition for that particular charge.

Undoubtedly, the zone previously called the true crater, and found by probing, is the extent of the zone of complete rupture. This does not fit with the definition of the true crater as being that zone from which material was completely disassociated from its previous position. The rupture zone is characterized not by this extreme movement, but rather by extreme breaking up and fracture together with much less mass motion or distances of movement.

Naturally, this rupture zone plays a part in terms of kinetic energy of the mass of earth moved by the explosion and, as such, should not be discounted in total-energy evaluation. The future study of this zone will be required to obtain a thorough understanding of cratering phenomena, and future developments in instrumentation technique will undoubtedly make such a study feasible.

It seems highly profitable, therefore, to examine the true crater, as defined by this discussion, and the results of these HE experiments to understand the comparative efficiencies of nuclear energy and HE for cratering purposes. Further, it is felt that this definition should be used in future cratering experiments in order to understand further the cratering phenomena.

Chapter 3

NUCLEAR PROGRAM

3.1 PROCEDURE

3.1.1 Colored Sand Columns. In preparation for TEAPOT Shot 7, twenty-one 8-inch-diameter vertical shafts were drilled along one diameter and through ground zero as shown in Figure 3.1. These holes varied in depth from 50 to 200 feet and were drilled with a wall-drilling rig of the calyx type, using driller's mud as the medium for carrying the cuttings to the surface. After the holes were drilled to the specified depth or greater, they were bailed dry and inspected for plumbness, diameter, and depth. Then, upon acceptance of a hole, it was immediately backfilled with the colored-sand mix.

All the holes were drilled to meet the specifications of the test plan, with the exception of Holes 1 and 8, which required re-drilling because of sluffing, and Hole 11, which was 20 feet short of 200 feet. Hole 11 was accepted, however, because it was determined that additional attempts to obtain the 200-feet depth might cause the entire lower section of the hole to collapse. Figure 3.2 shows the drill rig over Hole 14.

After the 21 holes were backfilled with the colored-sand mix, the ground was graded with a motorized grader, and the positions of the tops of the columns were surveyed. Specifications for the finished columns are given in Table 3.1.

The sand for the columns was mixed with the water-base paint by use of a portable cement mixer. Soil from the test area was first sifted through a 2-inch-mesh screen and then shoveled into the mixer. The bulk water-base paint was first diluted with approximately three parts of water to one part paint and then slowly injected into the mixer to obtain a uniform mix. The required uniformity of sand-to-paint was easily obtained by controlling the number of shovels of sand and gallons of paint per mixer load. After thoroughly mixing the sand and paint, the mixer load was dumped into the hole through a large metal funnel, and measurements of the height of fill of each load were taken to ensure that no appreciable sluffing of the walls or bridging of the mix had occurred. Figures 3.3 and 3.4 show the mixing and backfilling operation in progress. Figure 3.5 shows a sample of a mixer load being removed from the mixer and preserved in a glass jar for future reference as to color or uniformity of the entire column.

3.1.2 Aerial Markers. It is impossible to obtain crater measurements by surveying at early times after an underground nuclear burst because of the high residual-contamination field in and around the crater and lip area. To overcome this difficulty, aerial mapping procedures were used on Shot 7 to obtain early-time profiles of the

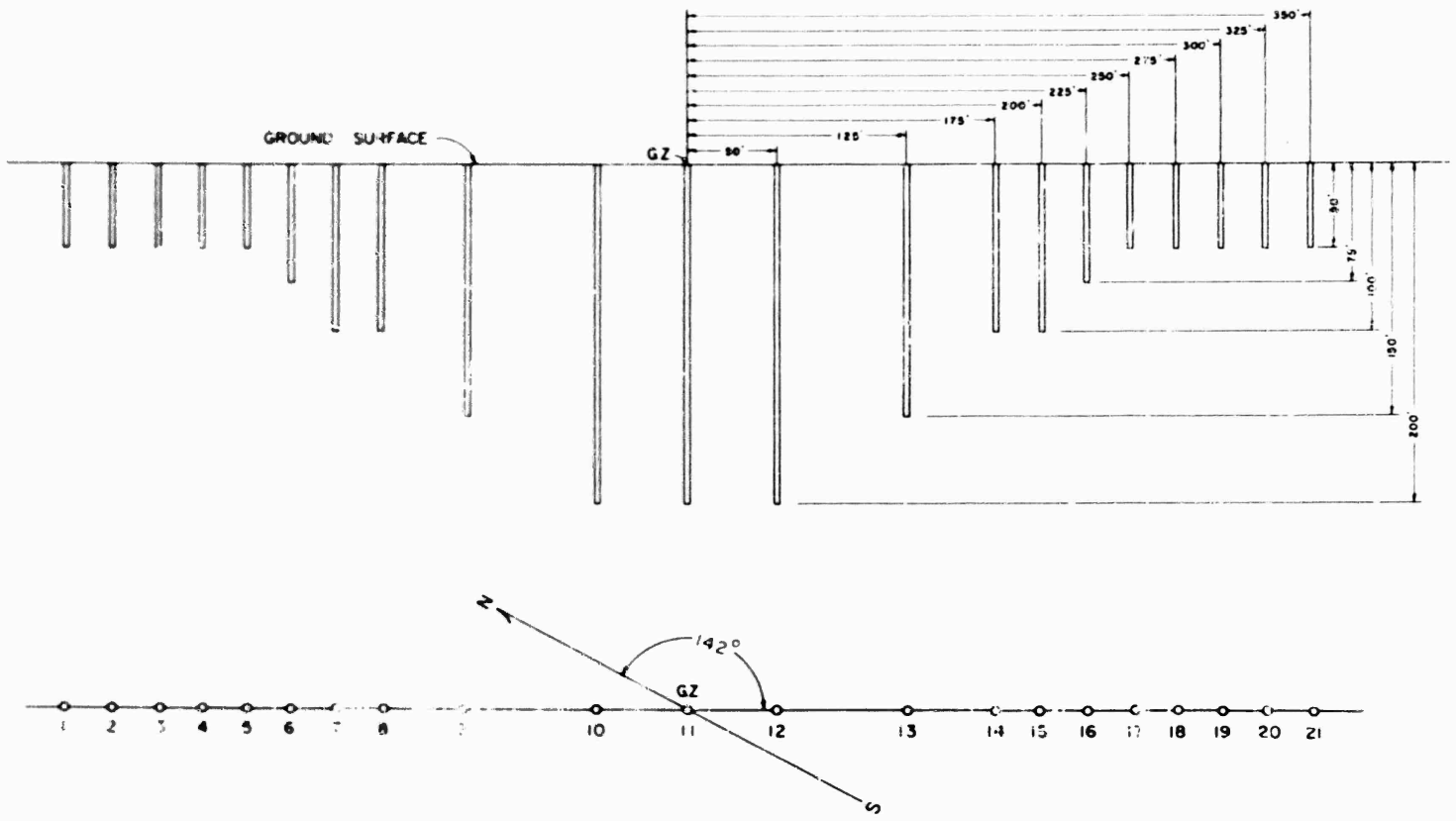

Fig. 3.1 Layout of Colored Sand Columns for Shot 7

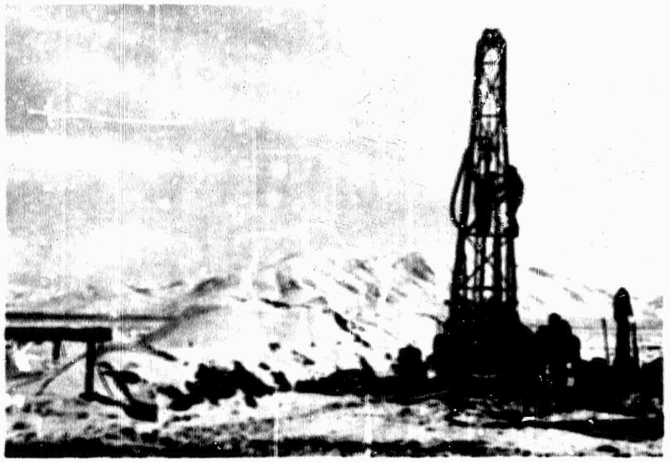

Figure 3.2 Drill Rig in Position over Column No. 14 at 175 ft from Ground Zero.

Figure 3.3 Preparation of paint mix prior to mixing with sand in cement mixer.

Figure 3.4 Filling column with colored sand from cement mixer.

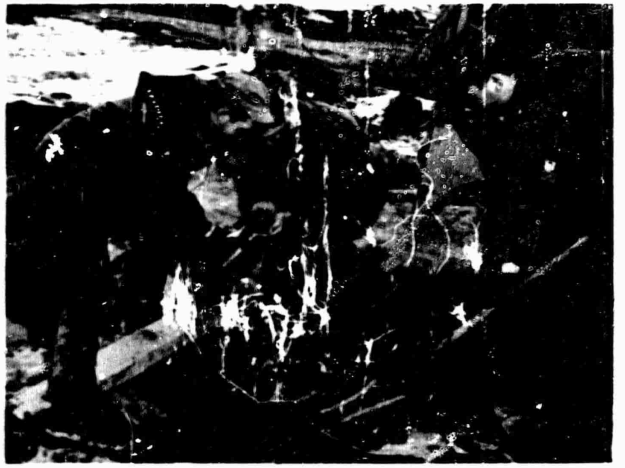

Figure 3.5 Taking sample of colored sand mix during column filling.

TABLE 3.1 - SPECIFICATIONS OF COLUMNS

Column Number	Color	Distance from GZ (ft)	Depth (ft)	Elevation Top Column (ft)	Elevation Bottom Column (ft)	Remarks
1	Red	345	54	4290.13	4236.13	This column was drilled 5 ft nearer GZ due to the failure of first hole to stand.
2	Yellow	325	49	4289.93	4240.93	
3	Black	300	51	4290.03	4239.03	
4	Red	275	51	4290.04	4239.04	
5	Yellow	250	52	4289.86	4237.86	
6	Black	225	82	4289.93	4207.93	
7	Red	200	104	4289.95	[illegible]	
8	Yellow	170	106	4289.90	4183.90	Column was redrilled 5 feet nearer GZ bec. the drill stem was lost in original hole; after recovery of same, uniformity of hole had been destroyed.
9	Black	125	163	4290.03	4127.03	
10	Red	50	214	4290.22	4076.22	
11	Yellow	0	206	4216.00	4082.00	
12	Black	50	216	4289.48	4073.48	At ≈125 ft from surface, an object, which appears to be a large stone, protrudes from side of hole and about halfway into hole.
13	Red	120	154	4289.85	4135.85	This column was redrilled at 5 ft nearer GZ because original hole was not plumb.
14	Yellow	175	109	4290.02	4185.02	
15	Black	200	113	4290.51	4177.51	
16	Red	225	78	4290.48	4212.48	
17	Yellow	250	62	4291.08	4229.08	
18	Black	275	55	4291.05	4236.05	
19	Red	300	64	4291.13	4227.13	
20	Yellow	325	60	4290.76	4230.76	
21	Black	350	59	4290.84	4231.84	

TABLE 3.2 - POSITIONS OF AERIAL MARKERS

Marker No.	Marker Elevation (ft)	Ground Level Elevation (ft)
1	4330.24	4329.24
2	4329.10	4328.10
3	4294.21	4293.21
4	4301.96	4300.96
5	4312.50	4311.50
6	4283.25	4282.25
7	4309.05	4308.05
8	4273.42	4272.42
9	4285.22	4284.22
10	4306.57	4305.57
11	4271.84	4270.84
12	4272.63	4271.63

crater and lip. Horizontal and vertical control for the aerial stereophotographs was obtained by placing aerial markers in 12 positions about ground zero, as shown in Figure 3.6. These markers were constructed of reinforced concrete in the form of a large cross (8 feet by 6 feet painted black and yellow), and after emplacement on the ground surface at the specified horizontal positions, their elevations were determined by survey. The horizontal and vertical positions of the markers are given in Table 3.2, and photographs of the markers and the emplacing techniques are shown in Figures 3.7 and 3.8.

3.2 RESULTS

3.2.1 Apparent Crater. By use of the aerial markers and mapping techniques described in Section 3.1.2, a contour map of the apparent crater and lip was obtained from aerial stereophotographs taken at H + 20.5 hours. Prints of these stereo pairs, taken at 3,130 feet above ground surface, are shown in Figure 3.9. The contour map obtained from these photographs is shown in Figure 3.10, and four profiles of the apparent crater and lip, running vertically through ground zero and at 0, 34, 90, and 138 degrees azimuth from true north, are given in Figures 3.11 through 3.14. From these four profiles the dimensions of the apparent crater were determined and are given in Table 3.3. For purposes of comparison, the dimensions of the JANGLE S and U craters are also given in Table 3.3.

3.2.2 Excavation of Sand Columns. Excavation work to uncover the colored sand columns could not begin immediately after the detonation of Shot 7 because of the very high residual-contamination hazard. Periodic checks were made on the contamination level in the crater and on the surrounding lip area at intervals of approximately two months to determine when the area could be entered in safety. During the summer of 1955 these checks indicated that decontamination work would be necessary if the excavation were to proceed during the calendar year 1955. Since this was felt to be desirable, a program was established to use land reclamation techniques to reduce the radiation hazard surrounding the crater to reasonable levels. This work was not AFSWP-sponsored and was conducted by personnel from USAERDL. It will be reported on in a report entitled, "Land Reclamation of a Crater Lip Area Using Earth Moving Equipment", to be published in the near future. Since the major portion of the excavation type work to be done in Area 10a was concerned with Project 1.6, it was decided to lump all similar work together under this project. Towards this end, the uncovering of the permanent displacement monuments under Project 1.7, the uncovering of JANGLE structures under Project 3.1.1, and the excavation down to original ground level and the cleaning out of structures 3.3/a-1 and a-2 were accomplished as part of the overall program.

To allow this work to proceed in orderly fashion, the first work done on Project 1.6 was to excavate down to the columns in the lip, i.e., above original ground level on the south line (Columns 13 through 21), and to make measurements of these columns. The work on

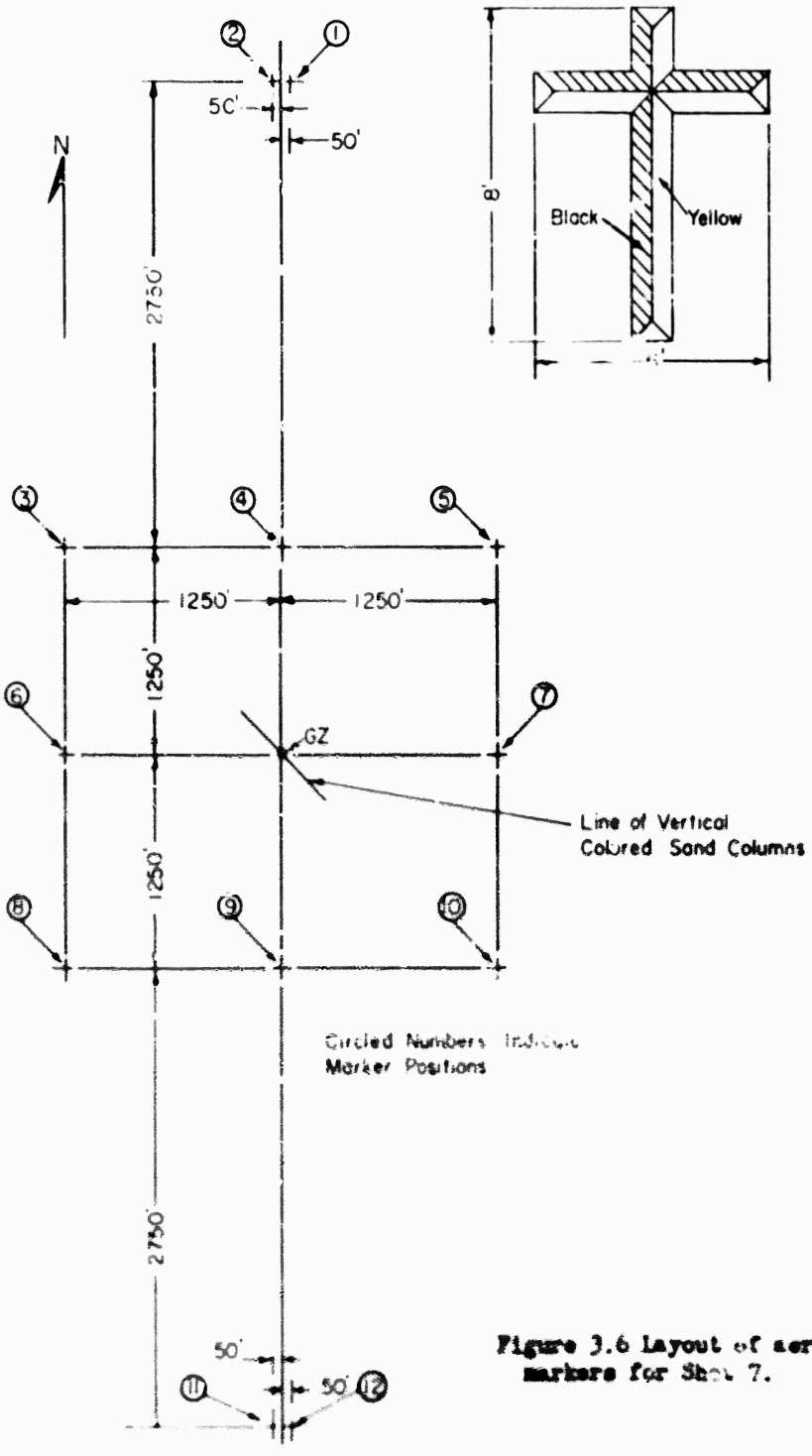

Figure 3.6 Layout of aerial markers for Shot 7.

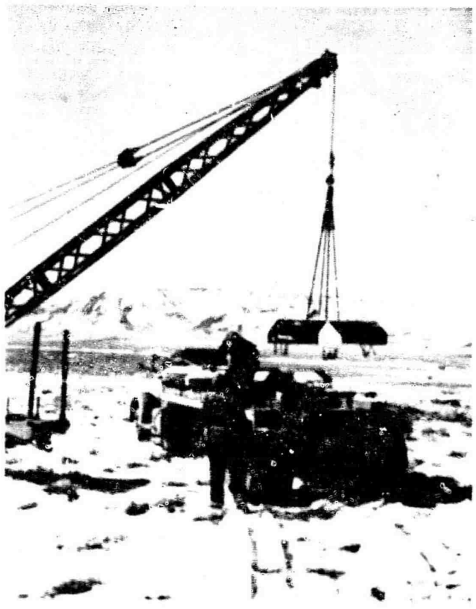

Figure 3.7 Precast aerial marker being removed from truck.

Figure 3.8 Positioning of aerial marker No 6.

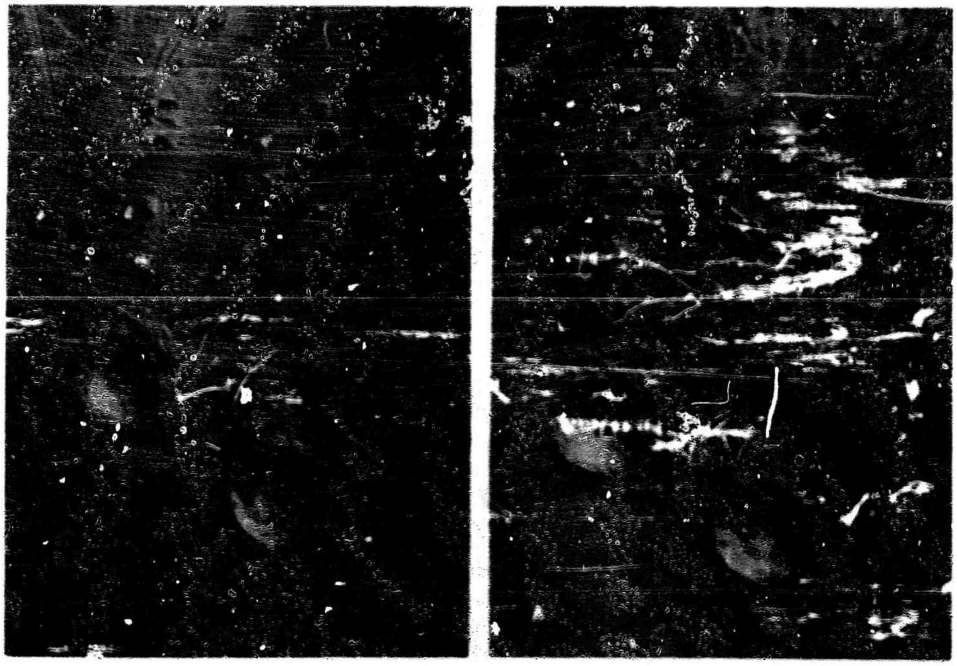

Figure 3.9 Aerial stereophotographs of the Shot 7 crater.

Figure 3.10 Contour map of Shot 7 crater and lip.

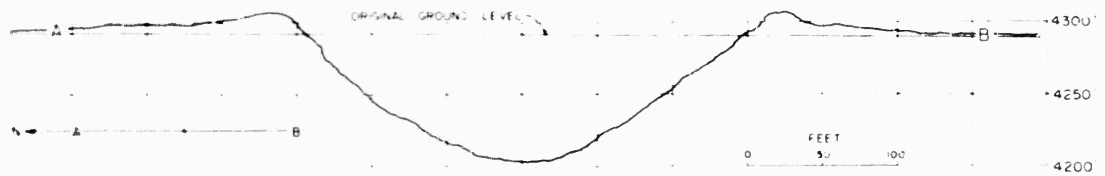

Figure 3.11 Profile AB of Shot 7 crater at 0° azimuth.

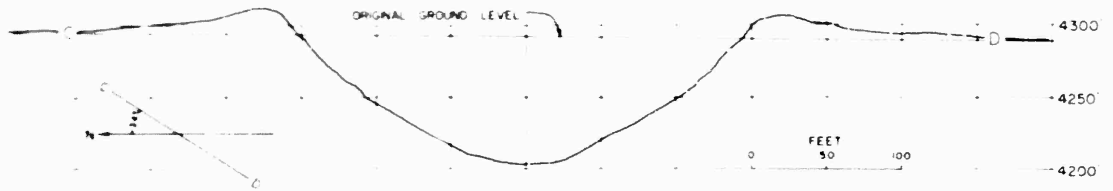

Figure 3.12 Profile CD of Shot 7 crater at 34° azimuth.

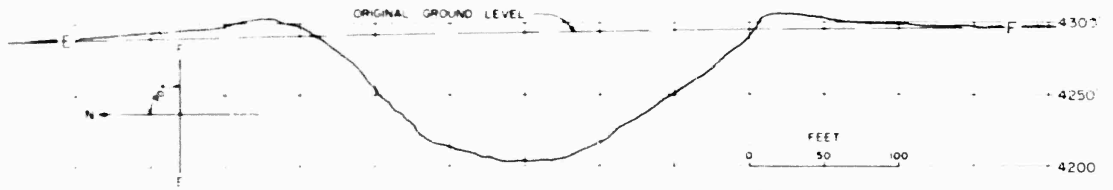

Figure 3.13 Profile EF of Shot 7 crater at 90° azimuth.

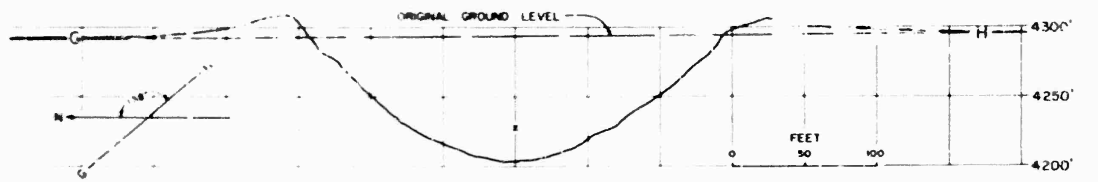

Figure 3.14 Profile GH of Shot 7 crater at 138° azimuth.

Project 1.6 then proceeded to the north line of the crater where no other programs had structures or excavation work requirements; in this area, work proceeded during that period of time in which the post-shot HE program under Project 3.3.2 was being carried out.

The extreme slopes on the side of the crater from Shot 7 were not predicted from previous HE work. Therefore, in planning the excavation work it had not been anticipated that ordinary earth moving equipment would be unable to negotiate the crater sides. A study of the proposed program indicated that all columns with the exception of these at ground zero and 50 feet to each side, i.e., No. 10, 11, and 12, would be in such a position that a trench could be dug to the west side of them allowing them to be uncovered with hand tools. This is basically the work that took place during the period 1 October to 5 November 1955. After an estimate of the difficulties involved in excavating to the center column was made, it was determined to defer this work until the spring of 1956 to allow time for planning a proper technique and letting a contract to accomplish the job.

The determination of an exact point in space of some portion of a column was accomplished by triangulation. A diagram of the method used is shown in Figure 3.15. Appendix A gives the data obtained by this method and the evaluations and the distances from a vertical center line through ground zero of significant measurements. These data have been plotted as shown in Figure 3.16. (see Figures A.1 and A.2, Appendix A, for detail on sand column movement.) Figures 3.17 through 3.43 give views of various stages of the excavation work and of the individual sand columns.

With the exceptions of Columns 10 and 12, those at 50 feet to either side of ground zero, all the columns were uncovered and documented. The various depths to which the columns were uncovered were dictated wherever possible by that depth at which it could be assumed that the column had suffered no shear or displacement of a magnitude of interest to the evaluation of the project. This depth, not including the center column, ranged from several feet at Columns 1 and 20 to about 45 feet below original ground level for Columns 7 and 13.

3.2.3 Interpretation of Sand-Column Data. The profile view of the crater as shown in Figure 3.16 indicates that some revision of the previously defined term "true crater" may be in order so that the zone of shear evidenced below the lip receives consideration. It is most likely that this zone of damage also occurs for smaller HE explosions but the dimensions of the resultant actual disturbances are so small as to go unnoticed. However, this ground movement can be both appreciable and important for underground explosions throughout the range of nuclear yields.

The top of Column 11, when uncovered, was 128 feet below the original ground level, or 61 feet below the center of gravity of the charge. This point was defined previously as being the depth of the true crater. It appeared obvious from the nature of the excavated soil

that all material directly above this point was in a zone of complete dissociation and had probably been ejected from the crater, but with insufficient energy to prevent falling back. This material was characterized by a much higher temperature than normal, although no exact measurements of this were made. Between 105 and 115 feet below

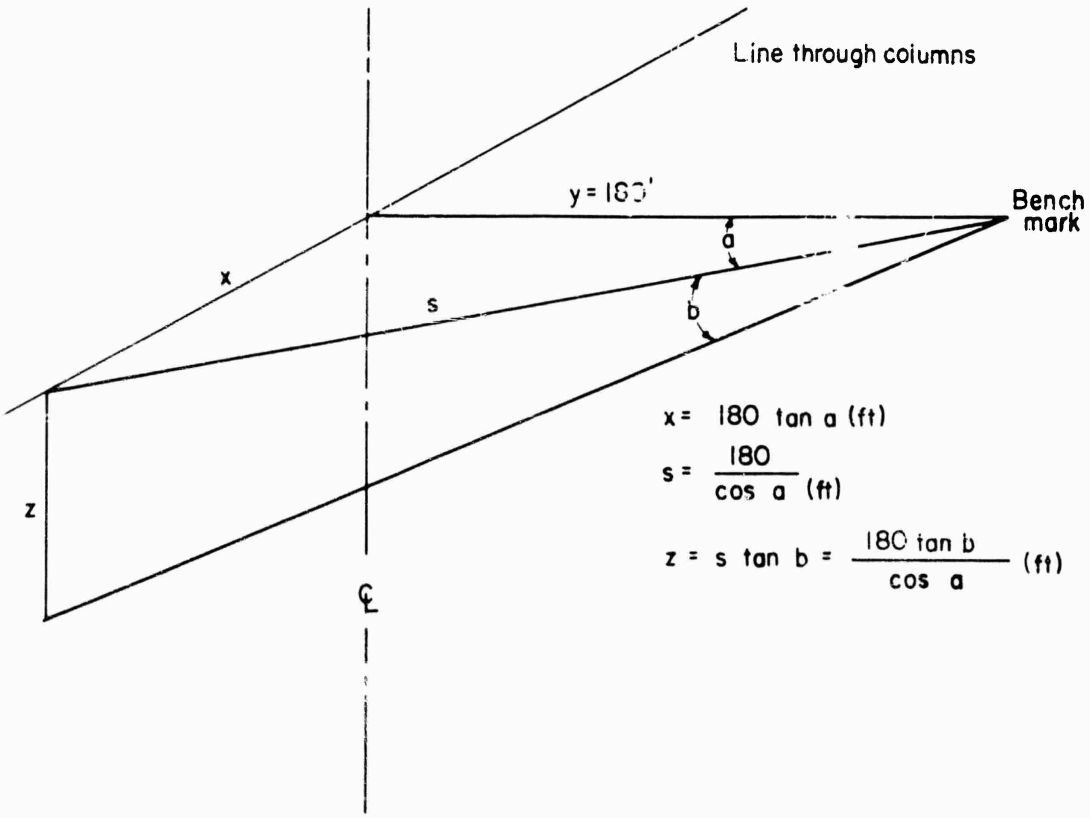

Figure 3.15 Method for determining point on each column.

the original ground surface, the residual radiation activity dropped quite rapidly to what was considered as only scatter from above.

Of particular interest is the action of the soil as evidenced by Columns 9 and 13 in the lip. The end of the trace of Column 9 extended outward to a greater radius than the end of Column 8. It appears that the ground movement which ultimately forms the lip close in to the edge of the crater is a sliding or shearing movement with that material which is closest to the burst point being given the greatest energy for this movement. The results of this movement are enhanced in the vertical direction by the compressive action of the shock in the rupture and plastic zones. This results in vertical displacement of the soil close to the crater since upward motion presents the path of least resistance to the compressed soil.

Evidence of the shearing action in the soil as a result of the radially expanding shock is shown quite clearly in Figures 3.30, 3.32,

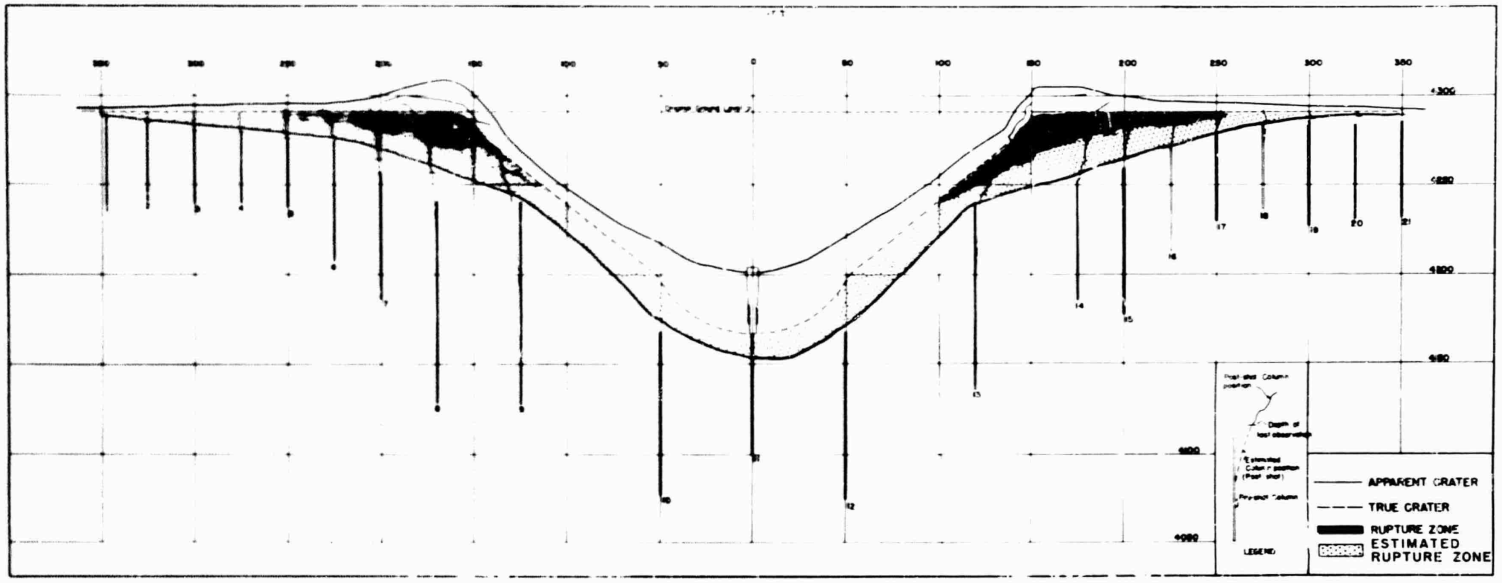

Figure 3.16 Profile of Shot 7 crater showing ground movement as measured by sand columns. For detial in shaded zone see figures A.1 & A.2.

Figure 3.17 View of excavation on South side of crater.

Figure 3.18 View of crater lip looking South through cut.

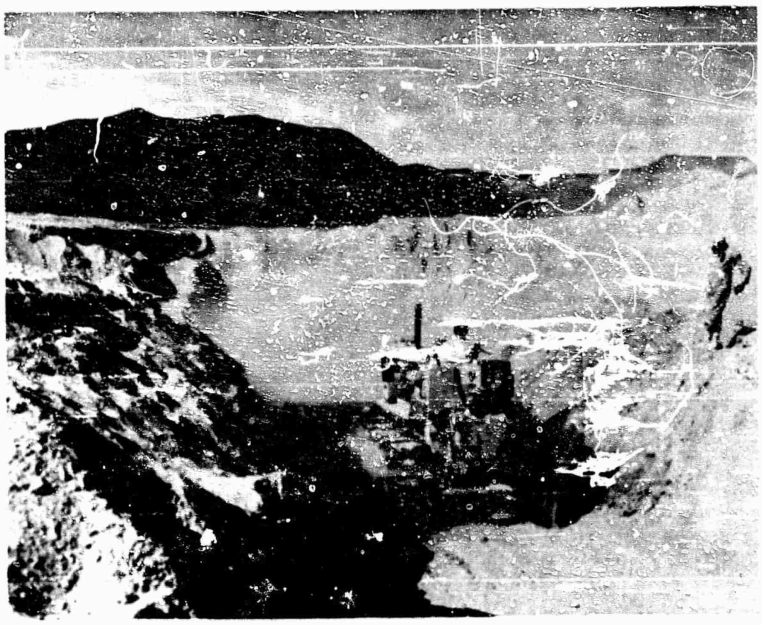

Figure 3.19 Dozer working in North lip.

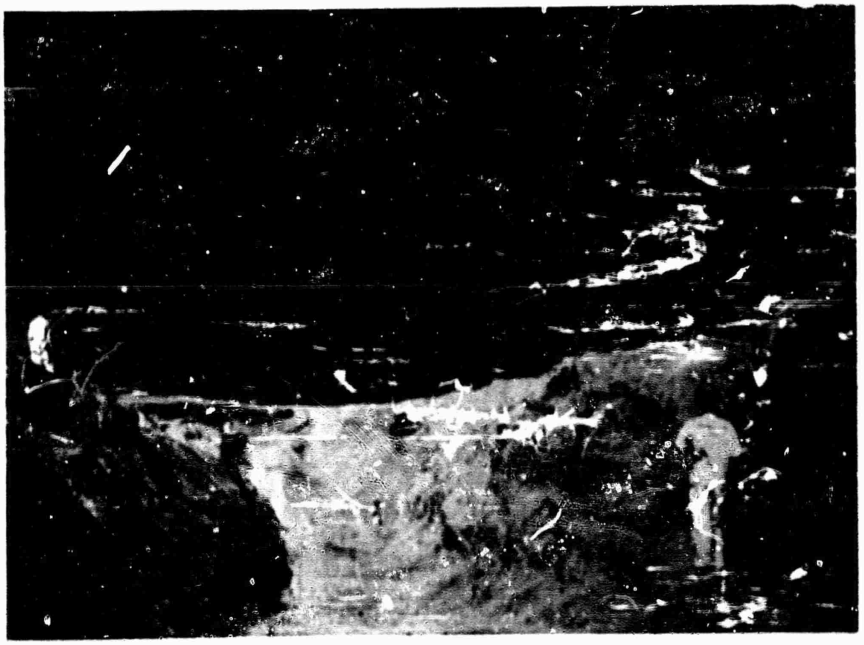

Figure 3.20 View of excavation work looking South through cut.

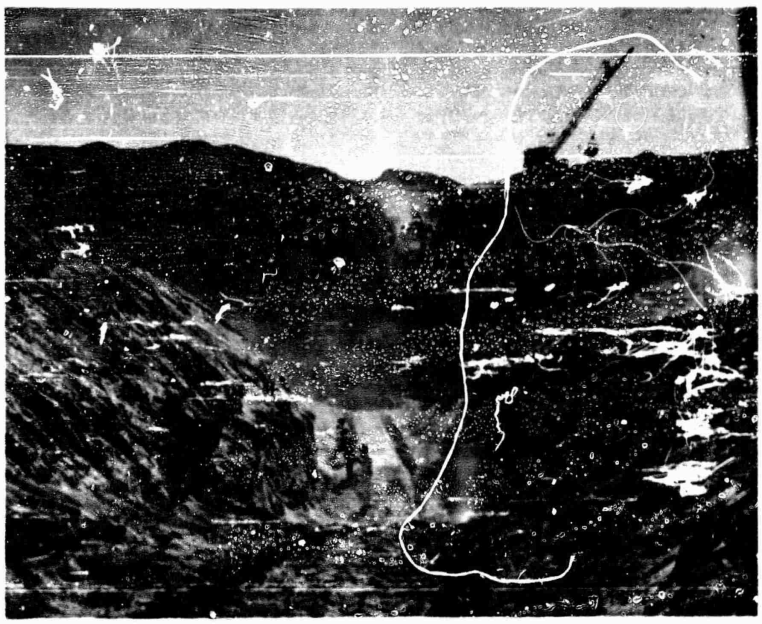

Figure 3.21 Excavation work, looking South.

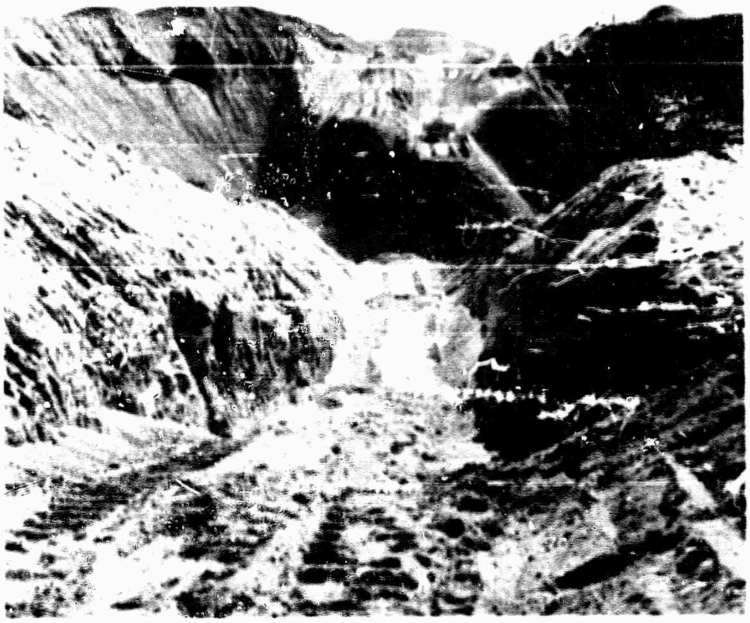

Figure 3.22 Excavation work, looking South,

Figure 3.23 Excavation work in North side of crater.

Figure 3.24 Excavation work in North lip.

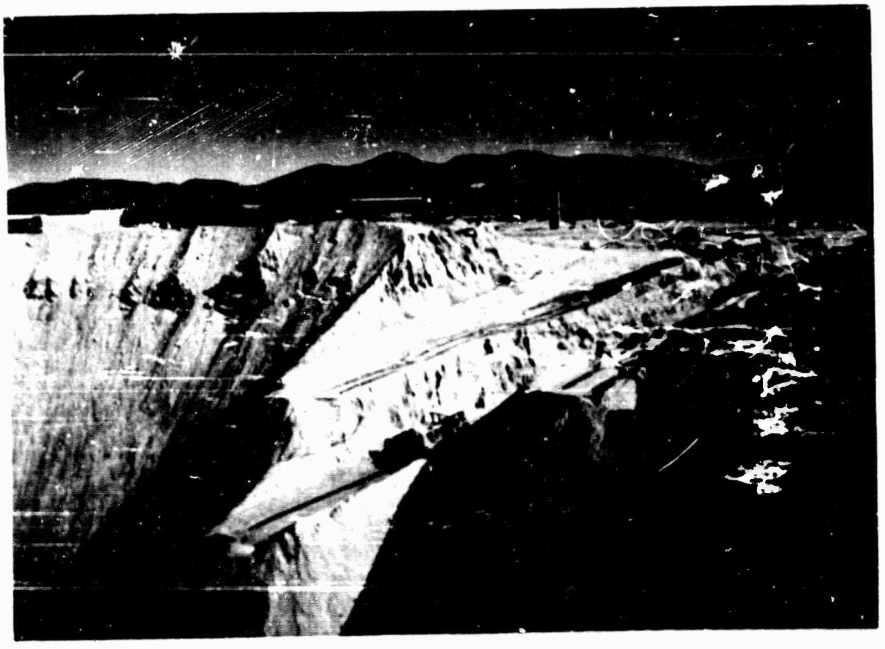

Figure 3.25 Dozer working in South side of crater

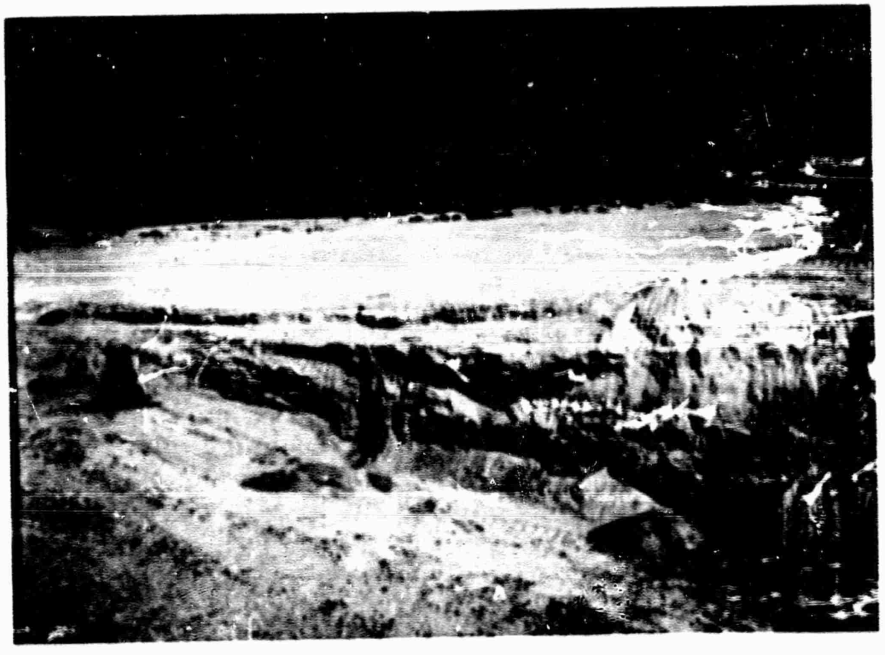

Figure 3.26 Column 3, 4, and 5

Figure 3.27 Column 3, Black

Figure 3.28 Column 4, Red

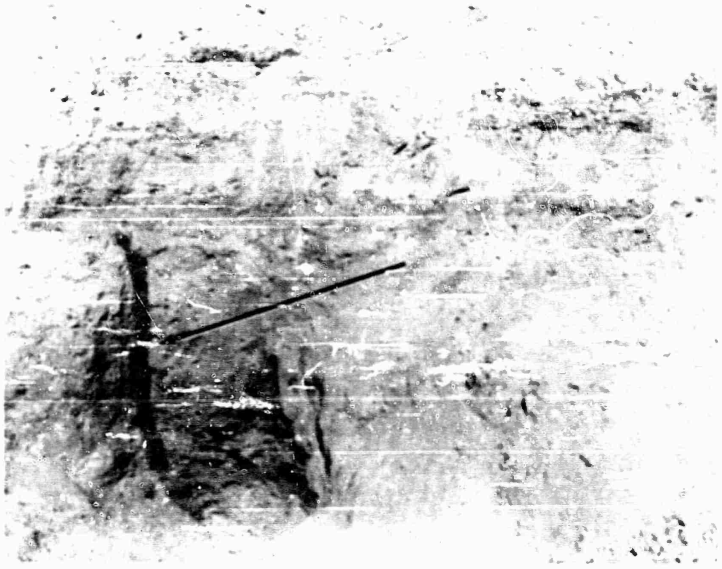

Figure 3.29 Column 6, Black.

Figure 3.30 Column 7, Red.

Figure 3.31 Column 8 in lip above original ground level.

Figure 3.32 Column 8, Yellow.

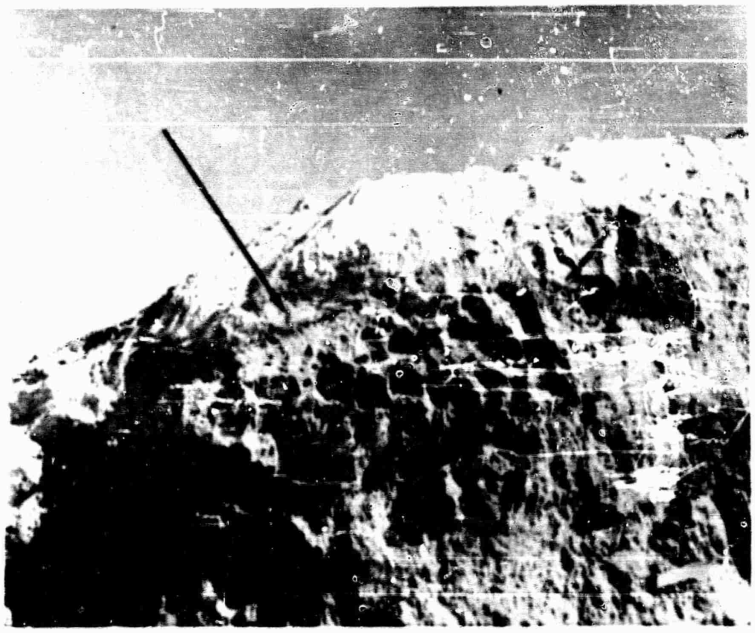

Figure 3.33 Column 9 in North lip.

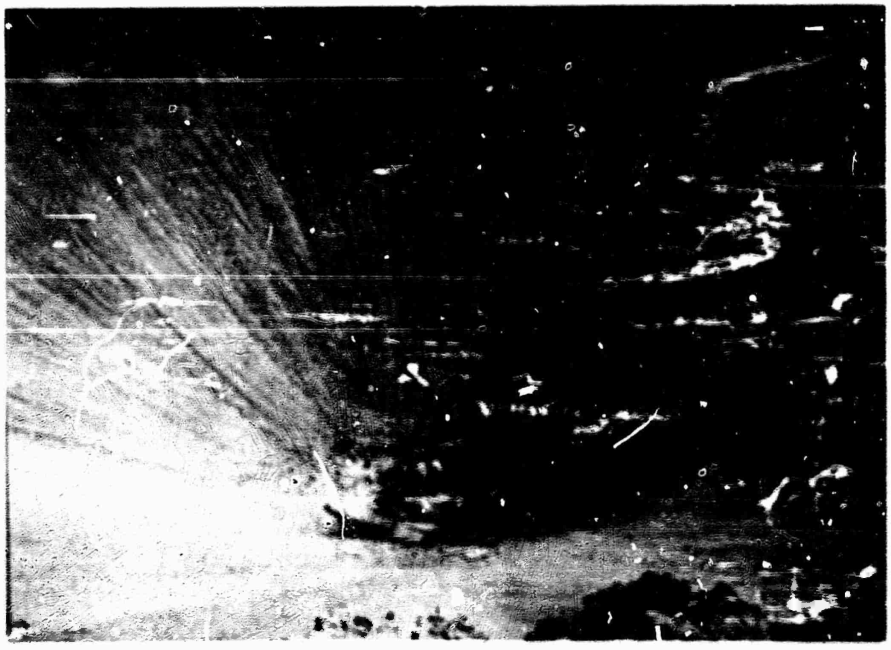

Figure 3.34 Hand excavation work on column 11 in bottom of crater.

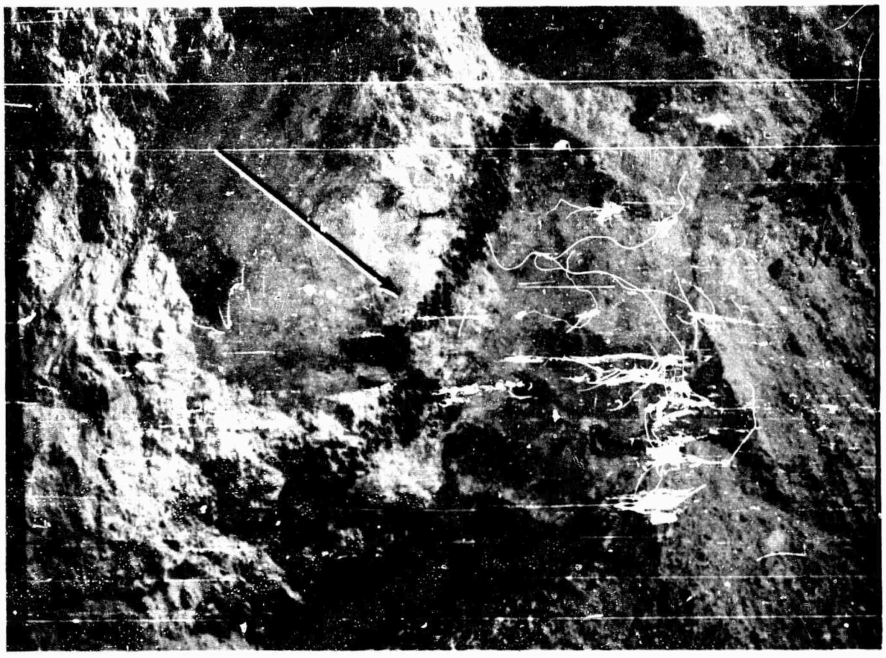

Figure 3.35 Column 13, Red.

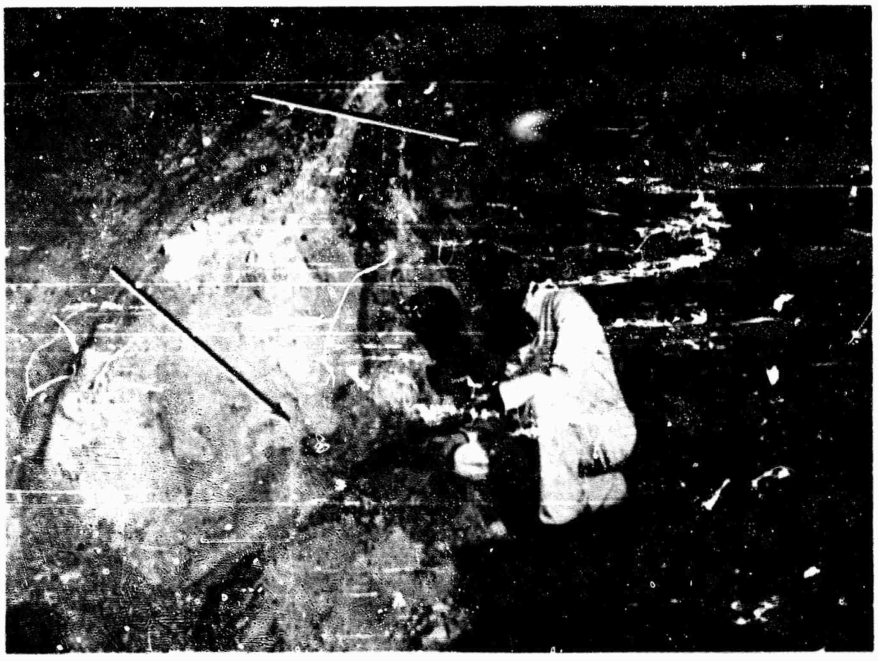

Figure 3.36 Column 13, Red in South lip.

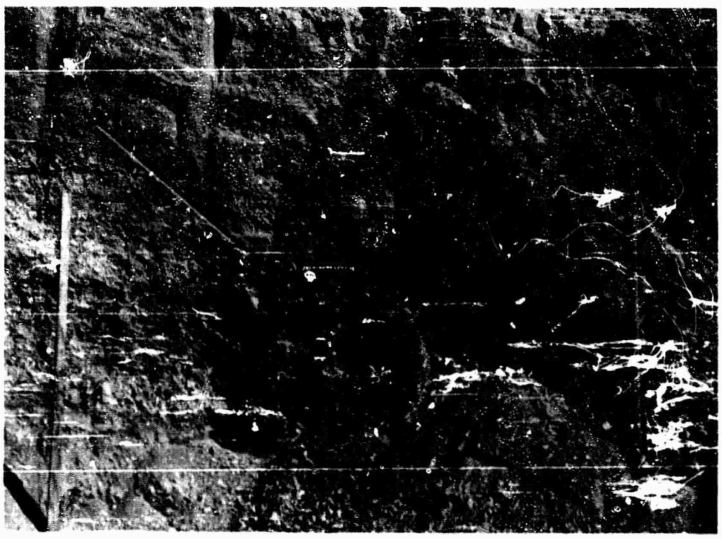

Figure 3.37 Column 14, Yellow.

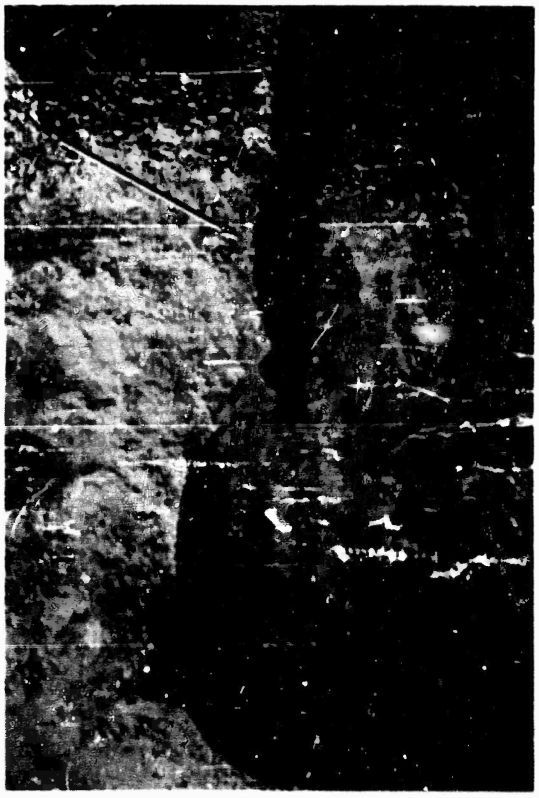

Figure 3.38 Column 15, Black.

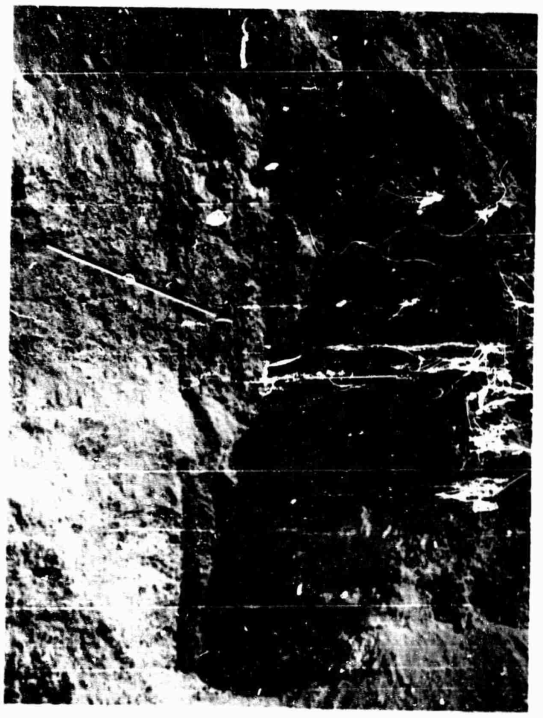

Figure 3.39 Column 16, Red.

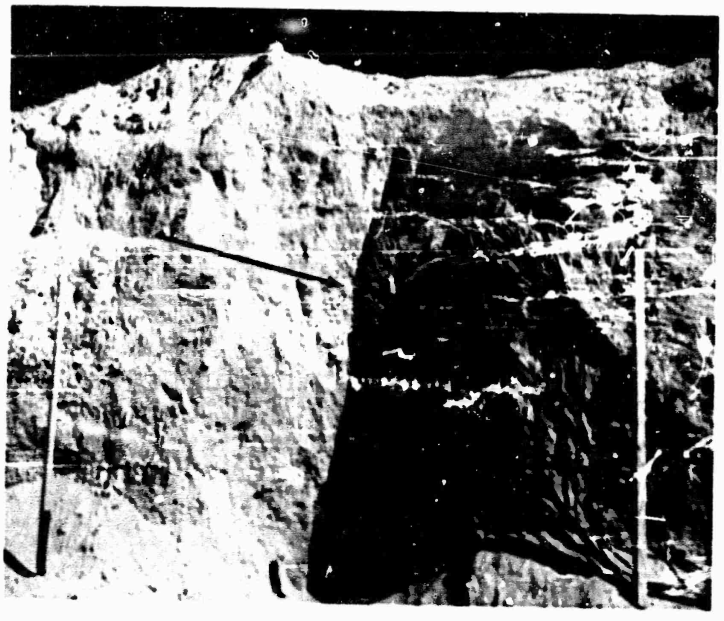

Figure 3.40 Column 17, Yellow.

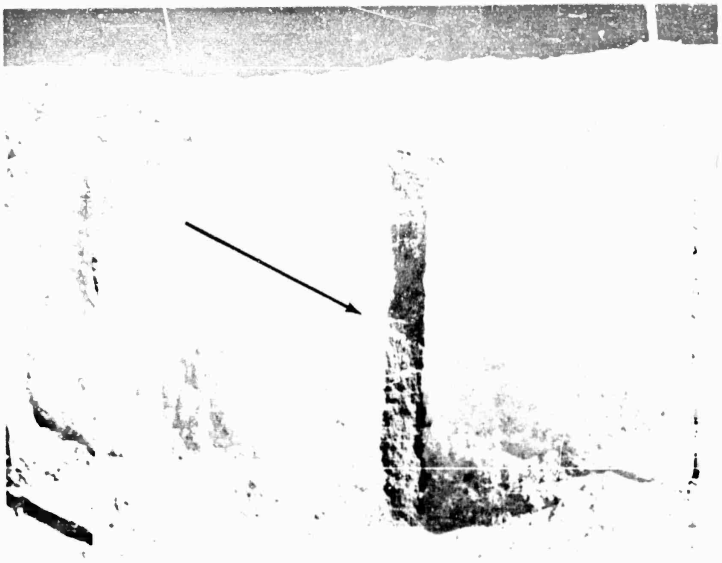

Figure 3.41 Column 18, Black.

Figure 3.42 Column 19, Red.

Figure 3.43 Column 20, Yellow.

3.38, and 3.39. This shearing action should be looked upon as being characteristic of the particular site of the explosion rather than as a measurement which will scale. The fact that it does occur is significant, and evidence points to this differential movement as being present in any nonhomogeneous medium such as soil.

The true crater dimensions for a 1.2-kt burst at a depth of 67 feet in a sand-and-gravel soil such as is found at the NTS are given in Table 3.4. They are based on the sand column measurements, and the somewhat revised definitions of the crater dimension terms, especially pertaining to nuclear bursts.

3.3 DISCUSSION

A most important consideration in studying the resulting crater from Shot 7 should be the relationship of these results to previous applicable tests, both HE and nuclear. In the section to follow, an attempt will be made to develop cratering curves for nuclear detonations in several soil types and to discuss the reliabilities of these curves, with respect to variations in medium as well as yield. There are large gaps still remaining in the knowledge concerning underground-explosion effects, and these appear to center about the problem of determining the early-time energy partitioning of the nuclear explosion in the various media. There is certainly some radius of development of shock from an underground explosion at which the medium will, disregarding magnitude, be unable to tell from what source the shock originated. However, within this radius and during the time which the energy is partitioning itself between such things as irreversible heating and the change of energy from a thermal to a blast state, there are many unknows. And, when an air-earth interface is interjected before such processes are completed, it further complicates the problem. Certainly there is a radius within which a nuclear explosion in soil or rock will be considerably affected as to energy partitioning by the presence of an air-earth interface. And, correspondingly, if the nuclear explosion were of small yield and were surrounded by a radius of air before encountering the soil, this would enter into the determination of the energy density of the explosion as it enters the work stage.

It has been shown by study and small-scale experiments in two programs at the Waterways Experiment Station that the cratering potential of an explosion is closely associated with the energy density of the explosive (References 4 and 5). These programs have shown that the crater is smaller when the energy density of the explosive is higher if the total energy release and the medium as well as the scaled depth of charge (as determined by total energy release and not charge weight) are held constant. The charges used in these two programs were 27 pounds of composition C-4 with an energy density of 780 cal/cm^3 and 54 pounds of 40 percent ammonia dynamite with an energy density of 1553 cal/cm^3.

For all of the shots detonated during these two programs at the Waterways Experiment Station, measurements were taken of the true craters as defined previously in this report, in the majority of the

TABLE 3.3 - APPARENT CRATER DIMENSIONS OF NUCLEAR BURSTS AT NTS

Dimension	TEAPOT Shot 7	JANGLE U	JANGLE S
Radius at Original Ground Level	146 ± 2 ft	130	45
Depth Below Original Ground Level	90 ± 1 ft	53	21
Maximum Lip Height	19 ft	8	---
Minimum Lip Height	7 ft	---	---
Radius to Maximum Lip Height	160 ft to 175 ft	---	---
Volume	2.6×10^6 ft^3	9.9×10^5 ft^3	4450 ft^3
Depth or Height to Center of Gravity of Charge	67 ft	17 ft	- 3.5 ft

TABLE 3.4 - TRUE CRATER DIMENSIONS

Depth below Original Ground Level	128 feet
Radius at Original Ground Level	150 feet
Volume of True Crater (Estimated)	3.25×10^6 ft^3
Radius to Significant Rupture (or Shear) at Original Ground Level	250 to 275 feet

TABLE 3.5 - CLAY CRATERING DATA FROM WES EXPERIMENTS USING 2½-lb SPHERICAL C-4 CHARGES*

Shot Number	Scaled Depth λ_c	Depth (ft)	Scaled Depth (ft/lb$^{1/3}$)	Radius (ft)	Scaled Radius (ft/lb$^{1/3}$)	Depth (ft)	Scaled Depth (ft/lb$^{1/3}$)	Radius (ft)	Scaled Radius (ft/lb$^{1/3}$)
EL-8	1.0	3.40	1.13	6.6	2.20	---	---	---	---
EL-13	1.0	4.40	1.46	6.7	2.23	[illegible]	2.13	7.5	2.50
EL-18	1.0	4.33	1.44	7.3	2.43	7.10	[illegible]	7.5	2.50
EL-23	1.0	3.90	1.30	6.7	2.23	6.65	2.22	7.0	2.34
EL-10	0.5	4.50	1.50	6.6	2.20	5.40	1.8[illegible]	6.6	2.20
EL-15	0.5	4.	1.40	6.4	2.13	5.50	1.8[illegible]	7.0	2.34
EL-20	0.5	4.00	1.33	6.8	2.26	5.55	1.85	7.5	2.50
EL-33	0.5	4.25	1.42	6.1	2.04	5.40	1.80	6.5	2.16
S-18	1.0	4.70	1.56	7.0	2.33	6.20	2.06	7.5	2.50
S-19	1.0	4.00	1.33	6.9	2.30	6.20	2.06	7.[illegible]	[illegible]
S-20	1.0	4.10	1.37	7.0	2.33	6.10	2.03	7.5	[illegible]

* References 4 and 5

instances by use of the sand column technique. The soil used for the programs was a lean clay of approximately 25-percent moisture content. The soil conditions throughout the tests were held as constant as was possible, with a pronounced effect in reducing scatter in the cratering data. Unfortunately for the present discussion, only two scaled depths were used, 0.5 and 1.0. However, even with this limitation, the significance of the findings concerning true crater depths and radii for the clay soil as compared with the MOLE 400 series shots in the NTS soil is important in indicating a range of values for true craters. Pertinent data from these programs have been extracted from the reports and included in Table 3.5. If the scaled true-crater depth values as given in Table 2.1 for the MOLE 400 series and in Table 3.5 for the WES programs are examined, it can be seen that for the given soil type and between λ_c values of from 0.26 to 1.0 the difference between this value and the scaled depth of burial of the charge remains nearly constant. This scaled difference (scaled true-crater depth minus scaled depth of burial) is an average value of 0.43 for the NTS soil and 1.21 for the WES lean-clay soil. A check with the Shot 7 results (using 100 percent TNT equivalence for scaling) gives a value of 0.45 for the same scaled difference.

The fact that this dimension scaled directly with HE is somewhat unexpected but can probably be explained by the following:

1. For any depth of burst for which the fireball does not vent the surface of the ground before shock breakaway, the distance from the center of gravity of the charge to the true crater depth should remain relatively constant for a given soil and yield.

2. The true crater depth defines a boundary of a certain shock strength and soil strength difference. This dimension will be dependent upon the shock transmission and soil strength characteristics of the various soil types.

3. For the true crater depth, the effects of inability to scale gravity and medium strength over a large range of yields could lead to a TNT equivalent value considerably higher than that determined by the apparent crater. The apparent crater, which is more directly associated with the kinetic energy imparted to the medium, should be less dependent on the scaling of gravity effects and material strengths.

These points are verified to a certain degree by the results of the ground-shock measurements for Shot 7 under Project 1.7 as reported on in Reference 6. The results of this project indicated higher earth accelerations, particle velocities, earth stress, and earth strain than would be predicted from the apparent crater radius.

3.3.1 Nuclear Crater Phenomena. It would appear profitable to examine in as much detail as possible the physical phenomena of cratering, especially with regard to those differences introduced by the use of nuclear devices versus high explosives.

One basic difference between these two is immediately apparent: the generation of the gas ball from which mechanical work is ultimately derived. For the purpose of discussing this point, effects beyond one charge radius (C_r) will be assumed independent of thermodynamic influences. One C_r is defined for HE as the radius of the inert charge. For nuclear devices it will be somewhere between the physical limits

of the device and the radius of a charge of HE of equal energy release, or more exactly, that radius where the transmission of energy by shock is faster than by radiation. The temperature at which this transmission occurs is estimated to be 300,000 Kelvin. The value C_T may differ for different soils or media and will not necessarily scale with yield according to $W^{1/3}$ because of the mass effects of the device itself.

TABLE 3.6 - ENERGY DENSITY COMPARISONS FOR 1.2-kt

Explosion	Assumed Charge Characteristics		Calculated Explosion Characteristics	
	Weight (lb)	Volume (ft^3)	C_T[a] (ft)	Energy Density at C_T (cal/ft^3)
TEAPOT Shot 7 fully tamped (1.2-kt)	8,000	16	4.5	1.1×10^5
JANGLE U in air space (1.2-kt)	8,000	16	6[b]	3.1×10^4

(a) C_T is the radius of the gasball when its temperature has cooled to 300,000 ° K.

(b) Assuming fireball as cube shape of emplacement room approximately 10 ft on side.

Therefore, a 1-kt device having a weight of 8,000 pounds could have a different charge radius than one weighing 800 pounds if for no other reason than the density of the bomb materials and the soil being different. However, this effect may be insignificant for fully tamped bursts since the densities of soil and the HE portions of the device would be comparable.

The energy densities of the JANGLE S, JANGLE U, and TEAPOT Shot 7 bursts under their respective environmental conditions are listed in Table 3.6. For purposes of comparison, C_T will be assumed to be the radius at which the temperature of the fireball is reduced to 300,000 degrees Kelvin. Also assuming that there is no electron stripping, and overlooking the feeding of radiant energy from the dense mass of the device to the shock wave, a rough approximation of energy density can be calculated as follows (Reference 7):

$$T \text{ (degrees)} = \frac{\text{Total Energy Release in Calories}}{\text{Grams of material engulfed times specific heat in cal/gm degrees}}$$

or, for TEAPOT Shot 7, temperature at breakthrough of case would be:

$$T = \frac{1.2 \times 10^{12}}{3.6 \times 10^5 \times 0.2} = 1.6 \times 10^6 \text{ degrees Kelvin,}$$

and, mass (M) of material in grams to reduce temperature to 300,000 degrees Kelvin would be:

$$M = \frac{1.2 \times 10^{12}}{3 \times 10^{5} \times 0.2} = 2 \times 10^{7} \text{ grams}$$

Therefore, the engulfed material for the three burst conditions listed in Table 3.6 would be, approximately: for TEAPOT Shot 7, 1.64×10^{7} grams of soil; and for JANGLE U, 1.64×10^{7} grams of air and soil (the grams of material less the weight of the device is $2 \times 10^{7} - 3.6 \times 10^{6} = 1.64 \times 10^{7}$ grams). The resultant calculations of energy density at C_r appear adequate for comparison purposes. Regardless of the inaccuracies in the calculations, they indicate that tamping, or conversely, air spaces, around the nuclear device can effect the energy density to a significant degree. In other words, if JANGLE U were detonated in a concrete room of approximately 1,000 feet^3 of air

TABLE 3.7 - TNT EQUIVALENTS FOR JANGLE U AND TEAPOT SHOT 7

Apparent Crater Dimension	Percent TNT Equivalent JANGLE U	TEAPOT Shot 7	Ratio of TNT Equivalents
Radius	37	21	1.8
Depth	64	39	1.6

space, as compared with Shot 7 which was carefully tamped with sand bags to avoid air spaces, then Shot 7 had an energy density at C_r of about 3.5 times that of JANGLE U. This information, coupled with previously described small-scale HE cratering experiments using explosives with an energy density ratio of two, gives reason to anticipate that Shot 7 should have a lower TNT equivalent for cratering than JANGLE U. The method for determining the TNT equivalents for JANGLE S, JANGLE U, and TEAPOT Shot 7 are shown in Figures 3.44 and 3.45. The 100 percent points are the actual nuclear data scaled on the basis of nuclear yield in pounds of equivalent TNT energy and the TNT curve is scaled from high explosive data on the basis of charge weight in pounds. The procedure is to hold the charge position and the crater dimension constant and vary the energy or weight of charge required to produce the given crater dimension. The point of intersection of a straight line from the origin, and passing through the 100 percent point, with the TNT curve gives the equivalent scaled TNT charge. Reference 11 can be referred to for illustrations of this method. Since the deeper scaled depth of burial would ordinarily be expected to give a higher TNT equivalent value for Shot 7, the lower values as shown in Figures 3.44 and 3.45 and Table 3.7 take on increased significance as to the effects of energy density on cratering. The ratios of the TNT equivalents in Table 3.7 are consistent enough to indicate that they are real differences.

The significance of these findings concerning energy density effects should next be looked at in terms of how they affect the prediction of cratering effects. Considering that an air space around the device is more significant than the mass-yield ratio in changing

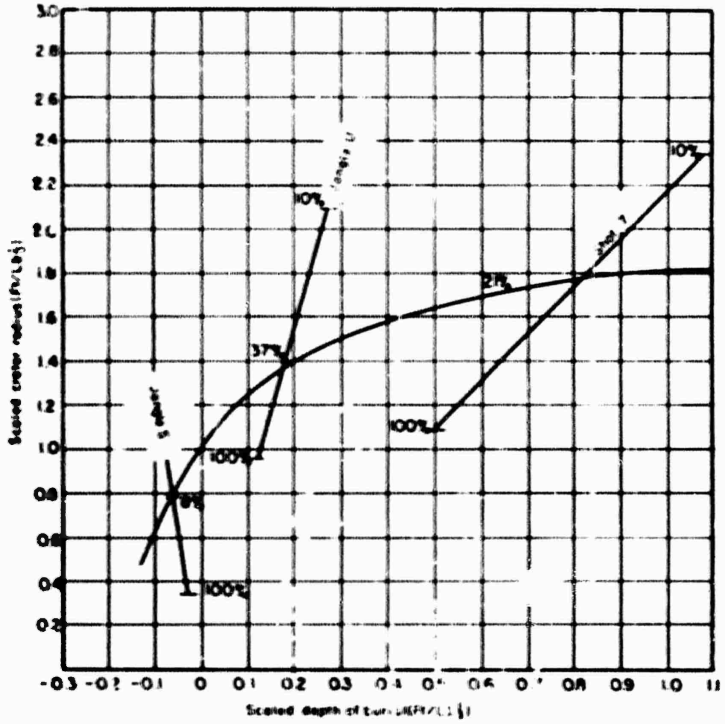

Figure 3.44 Scaled apparent crater radius versus scaled depth of burial showing TNT equivalent.

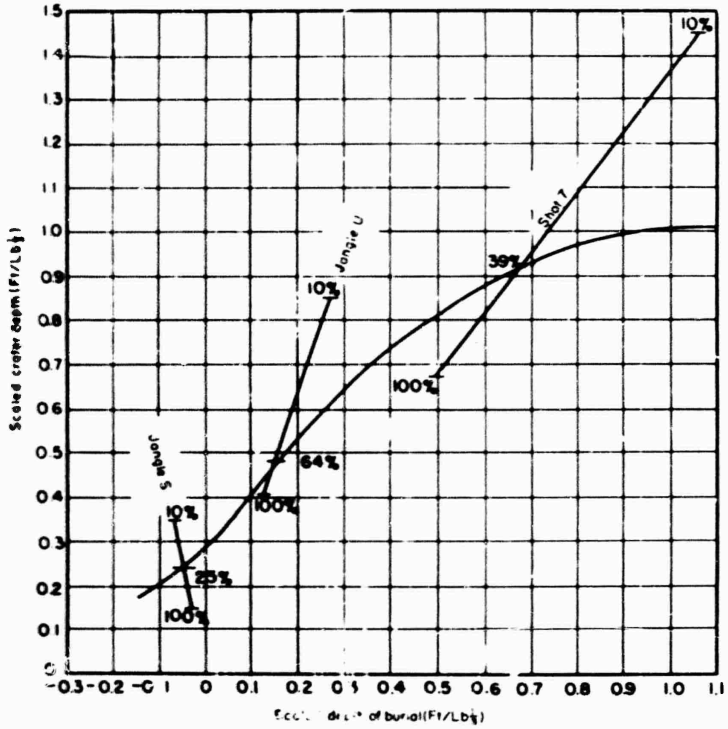

Figure 3.45 Scaled apparent crater depth versus scaled depth of burial showing TNT equivalents.

the energy density, it appears that the wisest step would be to interpret the data in terms of fully tamped charges. Further, until more is known about the effects of different mediums on early time radiative transport prior to reaching C_T, the effects of differing soil types on crater size can probably best be determined by comparisons of HE data in the various soil types. The calculation of nuclear cratering curves using HE curves for various soils and the TNT equivalents obtained from the fully tamped conditions of TEAPOT Shot 7 is indicated as next in the development of nuclear cratering curves for use by the various military agencies requiring such information. Subsequently, if better values of TNT equivalents for various media are determined, either by calculation or experimental observation, these curves can be adjusted accordingly. This course of action requires the following assumptions:

1. The charge is fully stemmed with no appreciable air space surrounding the charge.

2. When the charge is buried at any depth equal to or deeper than one C_T for a TNT charge equal to the nuclear yield in pounds, its TNT equivalent will be at least equal to those obtained for Shot 7 because of the high mass-to-yield ratio for that charge. This scaled depth is approximately $\lambda_c = 0.13$.

3. Beyond C_T for a given-yield nuclear detonation in a given medium, the medium will be unable to tell from what energy source the ground shock originated other than as shown by the velocity, amplitude, and duration of the shock, and attenuation of the shock beyond C_T will be almost entirely dependent on the characteristics of the medium.

4. The use of a TNT equivalent versus charge position curves as given in Figure 3.46. These curves are based on the arguments previously presented in this section (3.2.3).

It is possible that a misunderstanding of the effects of energy density on TNT equivalent can lead the reader to presuppose, from assumption three above, that the general behavior or thermodynamic state of the nuclear gas bubble at C_T is the same as for a high explosive detonation. Chronologically, the mass of the device and the medium immediately outside its case determine C_T which then determines the energy density at shock breakaway. The energy density thus determined defines such shock parameters as density, material velocity, and pressure at breakaway. These initial configurations of density, material velocity, and pressure are subsequently attenuated to various degrees by the shocked medium; however, their initial values largely determine the partitioning of energy between waste heat and kinetic energy at breakaway. Energy density, as used here, applies only to conditions at breakaway, or C_T. If all energy dissipation is accounted for, C_T for a nuclear explosion could never be as large as the charge radius for an equal energy release of high explosive. Unfortunately, the numerous difficulties of such exact calculations of energy

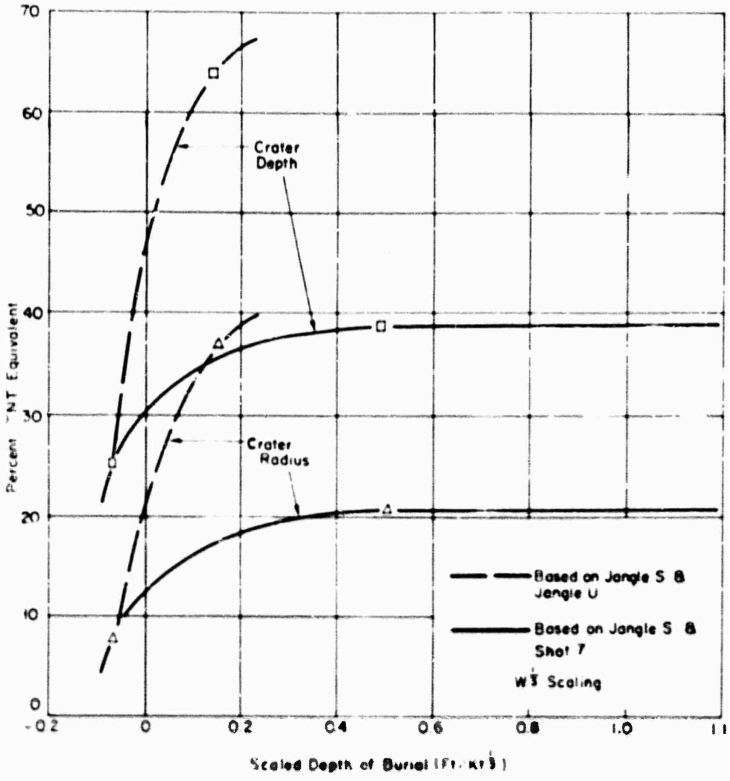

Figure 3.46 TNT equivalent versus depth of burial for 1-kt (nuclear) explosions of different energy density.

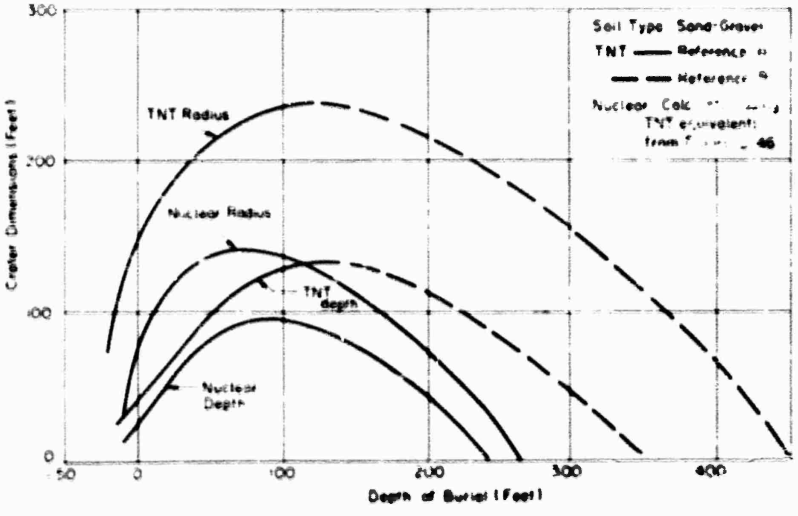

Figure 3.47 Crater dimensions for 1-kt of either HE or nuclear in sand-gravel soil type.

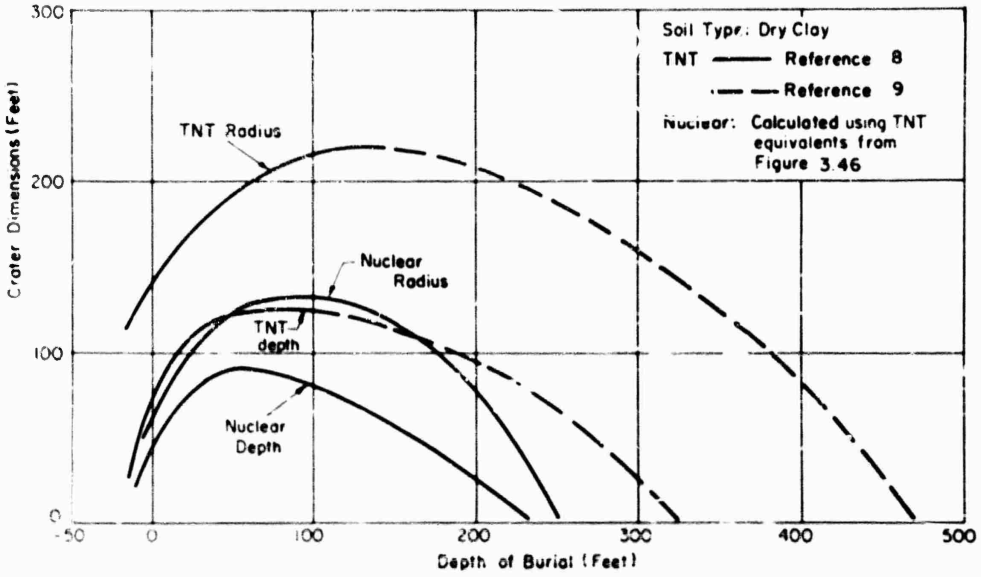

Figure 3.48 Crater dimensions for 1-kt of either HE or nuclear in dry clay soil type.

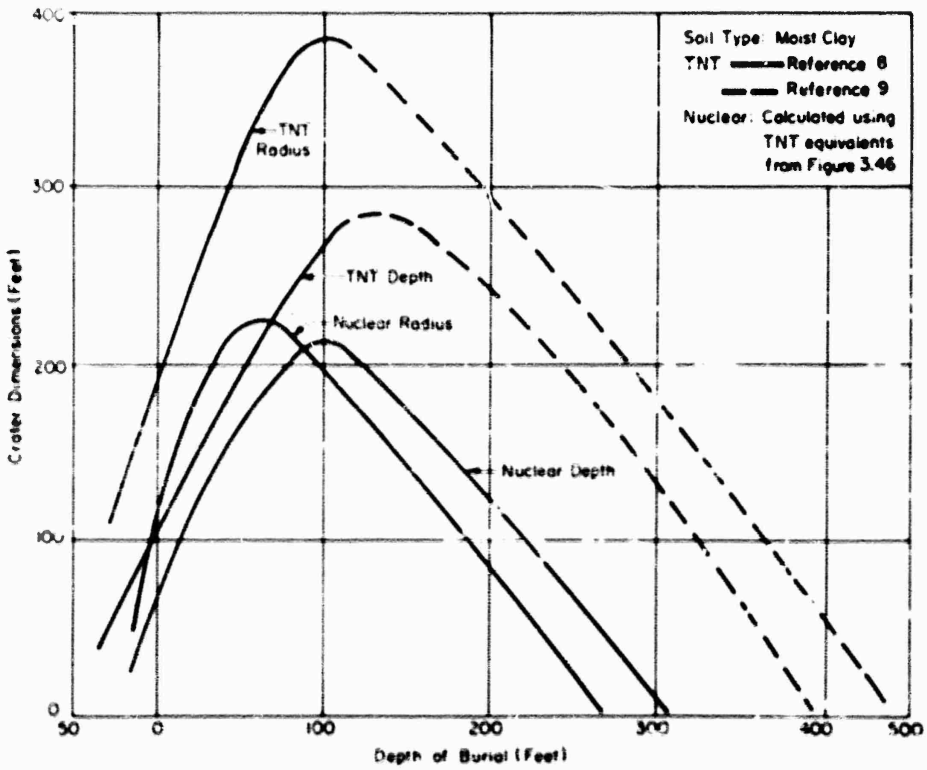

Figure 3.49 Crater dimensions for 1-kt of either HE or nuclear in moist clay soil type.

dissipation have not yet been overcome. Consequently, the C_r values calculated for JANGLE U and TEAPOT Shot 7 are used for comparison purposes only and are considered reliable for indicating differences in energy density at breakaway but not exact quantities.

3.3.2 Nuclear Explosions in Various Soils. The results of this project should be applied to soils other than those found in the NTS. One of the best available compilations of information on cratering effects from HE is available in the final report on Project MOLE. (Reference 8). The values of scaled apparent-crater radius and depth

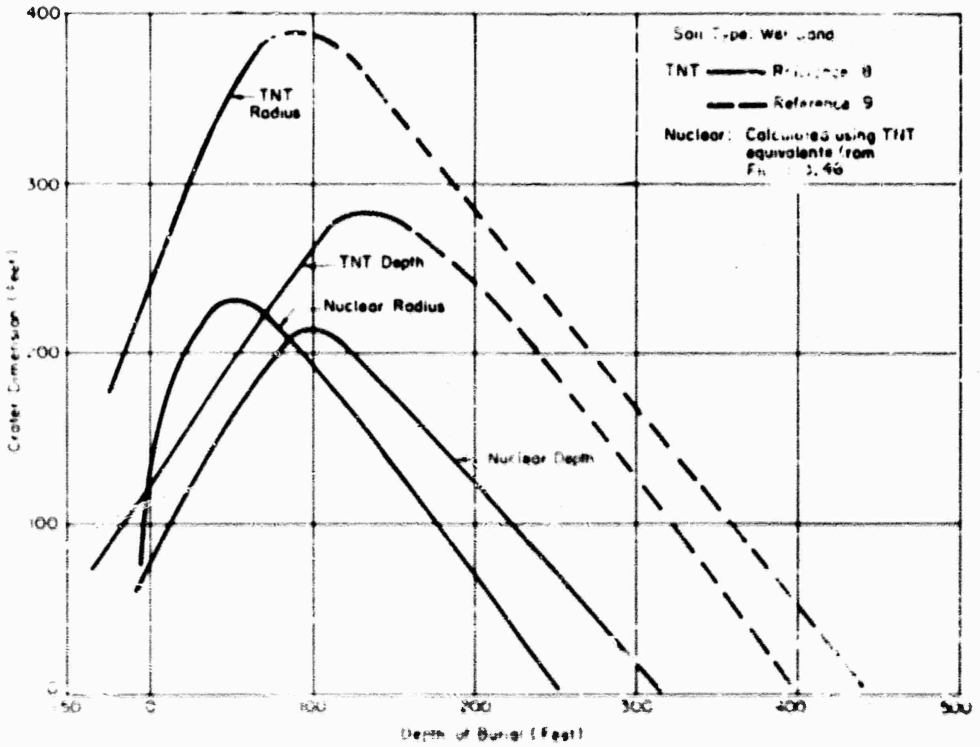

Figure 3.50 Crater dimensions for 1-kt of either HE or nuclear in wet sand soil type.

for sand and gravel, dry clay, moist clay, and wet sand as shown in Figures 8.112 and 8.113 of Reference 8 will be used here with one exception; that of apparent crater depth for sand and gravel, for which the curve from Figure 2.20 of this report will be used. These cratering curves were used along with the TNT equivalent values for fully tamped charges from Figure 3.46 to plot the nuclear-charge cratering curves given in Figures 3.47, 3.48, 3.49, and 3.50. The solid lines from Figure 3.46 were used for the TNT equivalent values, since as discussed in Section 3.3.1, the JANGLE U burst cannot be considered a true underground burst because of its somewhat special burial configuration. Therefore it should not be used for extrapolation

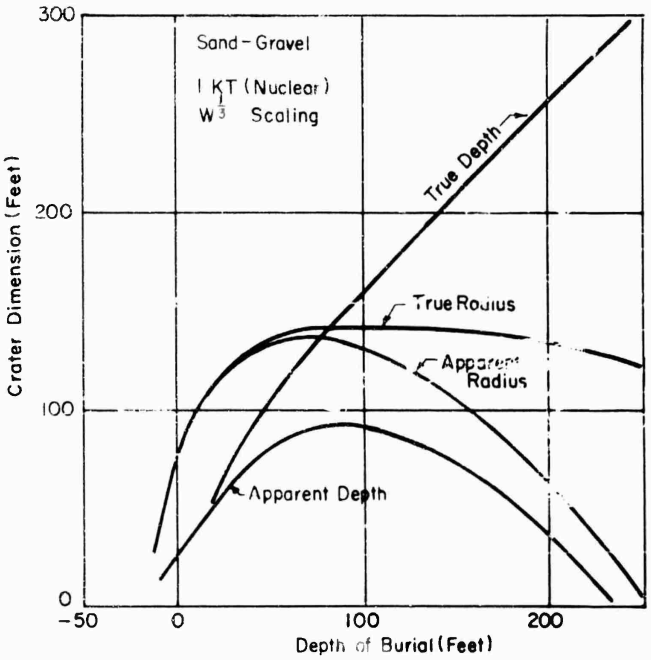

Figure 3.51 Crater dimensions for a 1-kt nuclear burst in sand-gravel soil type.

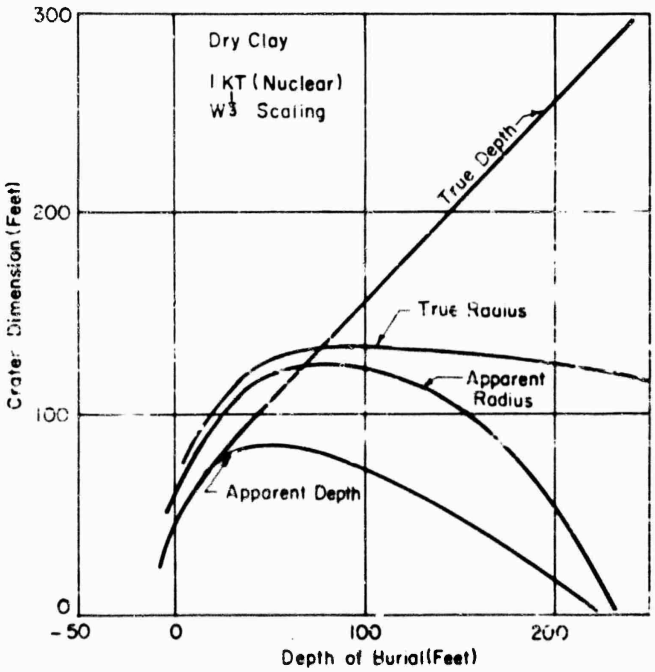

Figure 3.52 Crater dimensions for a 1-kt nuclear burst in dry clay.

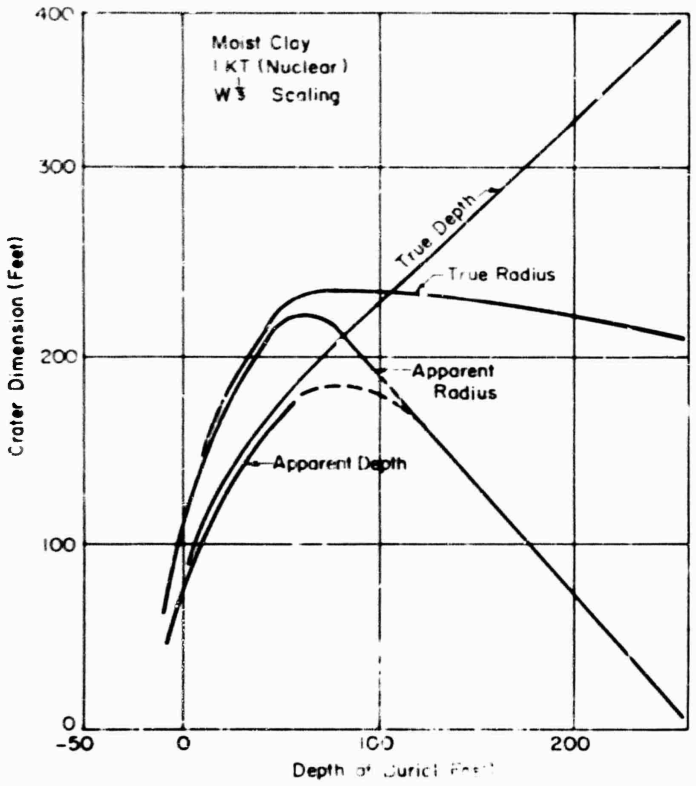

Figure 3.53 Crater dimensions for a 1-kt nuclear burst in moist clay soil type.

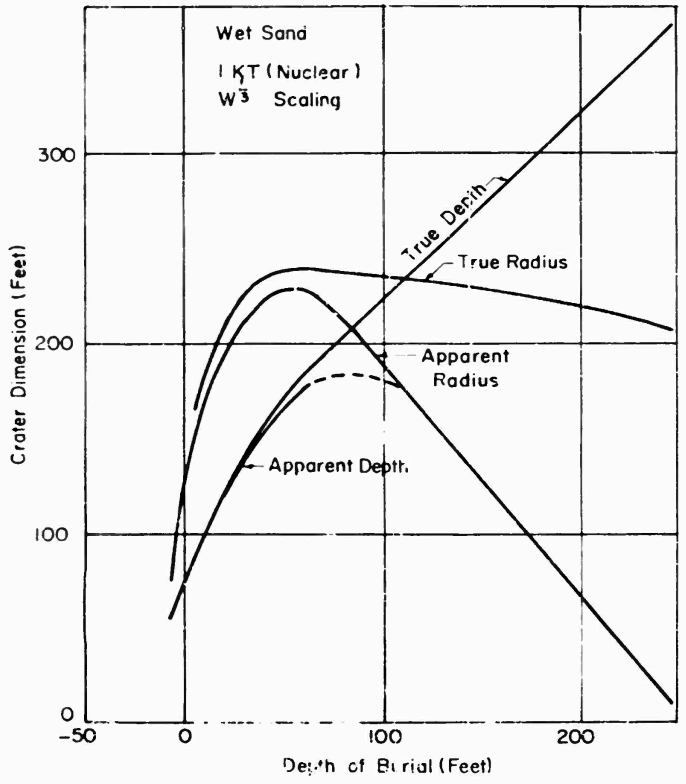

Figure 3.54 Crater dimensions for a 1-kt nuclear burst in wet sand soil type.

purposes to other yields and soil types. This is not meant to imply that the JANGLE U burst configuration might not be highly desirable under certain circumstances in order to increase the TNT equivalent.

Because the TNT equivalence of a subsurface nuclear explosion will be dependent upon the energy density of the explosion when its radius is C_r, it would be incorrect to assume that the TNT equivalents given in Figure 3.46 will hold for all burst configurations. The assumption will be made that they hold for fully tamped bursts in soil. However, when a better understanding of the effects of energy density at shock breakaway, or C_r, on TNT equivalent is developed, the weapon-effect information should be suitably corrected. In this way, some portion of the so-called scatter in the data may resolve itself into real differences.

In order to extend the cratering curves out to a scaled depth of burial where no apparent crater occurs, it was necessary to go beyond the data available from the MOLE programs. A survey of the available information indicated work by the British (reported in Reference 9) was probably a best estimate of the positions of the curves beyond a scaled depth of about 1.0. This work was also in good agreement with the work in this country of a similar nature (reported in Reference 10), namely the use of penetration bomb explosions of various sizes to indicate scaled crater dimensions with a correction for various charge-weight to bomb-weight ratios.

The relatively large difference in TNT cratering equivalent values for apparent radius (21 percent) and apparent depth (64 percent) led to a problem in constructing the nuclear curves in Figures 3.49 and 3.50; namely, the depth was a larger dimension than the radius. While it is reasonable to expect that this condition might exist at some instant immediately after the burst, it would most certainly dissappear as a result of the natural angle of repose of the sides of the crater. It should not be expected that this would ever exceed one to one. Therefore, the nuclear depth curves have been reduced in Figures 3.49 and 3.50 to coincide with the nuclear radius curves. This seems a reasonable reduction, since a small increase in crater radius from sluffing in of the crater sides would produce a relatively large decrease in crater depth.

Regarding the apparent crater radius curve for wet sand, the effects of subsidence at the surface of the ground for charge depths not expected to give apparent craters would give a dish-shaped appearance; however, this effect has not been included in the curves of Figures 3.50 and 3.54.

The method which is used in TM 23-200 for prediction of apparent crater sizes in other than sandy gravel soils (the use of soil factors) does not appear to be in any serious disagreement with the results of this project for depths of burial down to $\lambda_c = 0.5$. The difference in the crater dimensions for the different soils is nearly a constant between the surface of the ground and scaled depths of about $\lambda_c = 0.5$. However, it is felt that there would be a decided advantage to the use

of separate curves for the soil types on which good information is currently available, because the soil factors do not remain constant beyond $\lambda_c = 0.5$ and are not necessarily the same factor for HE and nuclear at a given depth value. Therefore, the soil-factor method of presentation of crater dimensions in various soil types has not been used in this report. For the prediction of true crater dimensions, the soil factor as used in TM 23-200 is not applicable.

The determination of the true-crater radii and depths for nuclear bursts in various soils are based on the discussion from Section 3.3; these are presented in Figures 3.51, 3.52, 3.53, and 3.54. It is felt that the sand-gravel curves are the most reliable. The true depth curve for dry clay, moist clay, and wet sand are felt to indicate slightly small values; these curves should be revised accordingly as more HE data using the sand column techniques become available. The method used in construction of the true depth curves for the sand-gravel and dry-clay soils was to use a value of $\lambda_c + 0.45\ (1b)^{1/3}$ for $\lambda_c = 0.5$, and to have the true depth progressively increase from a value equal to the apparent depth at $\lambda_c = 0$ to 0.95 at $\lambda_c = 0.5$. The true-depth curves for the moist-clay and wet-sand soils were constructed in the same manner, using $\lambda_c + 1.0\ (1b)^{1/3}$ as the equation for the curve.

The use of soil factors for crater-dimension predictions, such as is used in TM 23-200, appear to be valid only between scaled depths of burial of from $\lambda_c = 0$ to 0.5, and only for apparent craters. It is concluded that separate curves are required for nuclear true and apparent crater dimensions in the soils examined, especially if the results are given for depths including camouflet depth.

Chapter 4
CONCLUSIONS

Considerable progress has been made toward developing methods for the prediction of craters from nuclear explosions in various soil types. A number of areas requireng more intensive study. However, the reliability of crater prediction has been considerably increased since the results of the JANGLE bursts were first published. The roles which energy density, energy partitioning, and variations in soil characteristics play in determining crater size are now more clearly understood, with a consequent reduction in data scatter.

From the tactical point of view, the apparent crater must still be reckoned with as a primary obstacle; its size and shape can now be more reliably predicted such that neither overdestruction nor failure to accomplish a mission will result. However, it is the true crater and in particular the true-crater depth that will be used for determination of the yield and depth of burial required for destruction of underground installations. It appears entirely feasible that deep underground targets can be destroyed by a proper selection of yield and depth of burst giving negligible undesirable surface effects and maximum sub-surface destruction.

The column technique has proven excellent for determination of the so-called true-crater dimensions and has allowed correlation between HE and nuclear data for the few soils in which the method has been used.

The apparent crater dimensions appear to be determined to a large degree by both the energy density and the energy partition of the explosion, even if the soil type remains constant. For scaled depths of burial of less than about 0.15 (or one charge radius as defined in Section 3.3.1), energy partition appears to play a more decisive role than energy density in determining the TNT equivalent of the explosion. However, if the explosion id depp enough to allow the shock to completely break away from the fireball before venting the air-soil interface, the energy density is the determining factor in establishing the TNT equivalent. Furthermore, the energy density can be appreciably affected by air spaces surrounding the JANGLE U burst considerably decreased its energy density at the time it entered into the work phase (or shock breakaway) and thus increased its TNT equivalent to about 1.7 times that for TEAPOT Shot 7, which was carefully tamped with sand bags. It is concluded that the TNT-equivalent versus scaled-depth-of-burst values as determined by Shot 7 should be used for prediction purposes until a more thorough understanding of the effects of air spaces on energy density is developed. Definitely, air spaces may be a desirable emplacement feature for maximizing of TNT equivalence.

The sand column data from Shot 7, when compared with the MOLE 400 HE series and with Waterways Experiment Station results in clay, indicate that for depths of burial greater than one charge radius the distance from the burst point to the depth of the true crater remains

essentially constant, dependent only on the yield and the soil characteristics. The results indicate that the true crater is primarily dependent on the shock transmission characteristics of the soil; whereas the difference between the apparent and true craters is determined by the kinetic energy imparted to the soil within the true crater volume. Thus, as the charge depth of burial increases, the depth of the true crater increases by this same amount; but the depth of the apparent crater decreases because of insufficennt energy for throw out of the material.

The difference between the true and apparent crater radii at the original ground surface is small for scaled depths of burial down to 0.75 or 1.0. But below these scaled depths it is felt that the true crater radius remains a relatively constant value until camouflet depth is reached.

No apparent crater will result for scaled depths of burial greater than about 2.0 to 2.5 for nuclear bursts which are fully tamped. This value will be increased somewhat for energy densities lower than that for Shot 7, but should not exceed a scaled depth of 3.0 to 3.5.

Camouflet depth should be relatively independent of soil type except for differences in soil density, since the apparent crater (or lack of it in this instance) depends primarily on the capability of the available energy for throwout to heave clear the soil mass over the charge.

APPENDIX A

SAND COLUMN DATA

Obs No	Horizontal angle from OZ (a)	Vertical Angle from Horizontal (b)	tan a	Cos a	Tan b	X (y tan a)	S (y/cos a)	Z (S tan b)	Transit Elev (ft)	Elev (ft)	Rod to Z (ft)
					Column 1						
1	62°36'00"	2°31'	1.929	.4602	.0439	347.25	391.13	17.19	4307.10	4289.91	---
					Column 2						
1	61°02'45"	2°42'	1.807	.4842	.0471	325.34	371.71	17.53	4307.10	4289.57	---
2	61°03'30"	2°46'	1.808	.4839	.0480	325.50	371.96	17.87	4307.38	4285.51	4.0
					Column 3						
1	59°03'30"	2°49'	1.668	.5141	.0492	300.26	350.08	17.22	4307.10	4289.88	---
2	59°07'00"	3°01'	1.671	.5132	.0526	300.95	350.67	18.48	4307.24	4285.76	3.0
3	59°05'45"	3°03'	1.670	.5136	.0532	300.70	350.46	18.67	4307.33	4282.66	6.0
4	59°05'00"	3°05'	1.668	.5140	.0538	300.36	350.16	18.86	4307.38	4281.52	7.0
					Column 4						
1	56°51'45"	3°00'	1.531	.5466	.0524	275.72	329.27	17.26	4307.10	4289.84	---
2	56°53'45"	3°03'	1.533	.5461	.0634	276.07	329.30	20.91	4307.24	4283.33	3.0
3	56°52'00"	3°07'	1.532	.5465	.0661	275.76	329.31	21.78	4307.33	4280.55	5.0
4	56°49'30"	3°11'	1.529	.5471	.0643	275.33	328.94	21.18	4307.38	4279.20	7.0
					Column 5						
1	54°24'45"	2°39'	1.397	.5819	.0462	251.53	309.30	14.32	4307.10	4292.78	---
2	54°24'00"	3°07'	1.396	.5821	.0895	251.42	309.21	27.69	4307.24	4279.55	---
3	54°22'30"	3°20'	1.396	.5824	.0934	251.28	309.07	28.80	4307.24	4275.44	---
4	54°19'00"	3°27'	1.392	.5833	.0954	250.65	308.58	29.44	4307.38	4275.94	2.0
					Column 6						
1	52°12'30"	3°04'	1.2[illegible]	.6127	.0535	232.12	293.73	16.74	4307.10	4291.36	---
2	52°42'30"	3°12'	1.[illegible]	.6058	.0559	236.35	297.09	16.61	4307.10	4290.49	---
3	51°42'00"	3°31'	1.[illegible]	.6197	.0672	227.91	290.42	19.54	3407.10	4287.56	---
4	51°3[illegible]'45"	3°47'	1.260	.6214	.0661	226.93	289.65	19.15	4307.10	4290.95	- 3.0
5	51°3[illegible]'00"	4°03'	1.262	.6209	.0789	227.23	289.89	22.90	4307.11	4284.21	---
6	51°33'00"	4°04'	1.259	.6218	.0842	226.69	289.46	24.39	4307.16	4282.77	---
7	51°34'30"	3°02'	1.258	.6221	.0880	226.49	289.30	25.48	4307.16	4281.68	---
8	51°31'30"	3°10'	1.258	.6221	.0904	226.49	289.30	26.16	4307.16	4280.00	1.0
9	51°30'30"	3°48'	1.257	.6224	.1015	226.35	289.20	29.35	4307.24	4276.86	1.0
10	51°33'30"	3°37'	1.259	.6218	.0983	226.62	289.48	28.45	4307.24	4278.79	1.0
11	51°28'00"	3°59'	1.256	.6230	.1048	226.08	288.92	30.30	4307.24	4275.94	1.0

Obs No	Horizontal Angle from GZ (a)	Vertical Angle from Horizontal (b)	Tan a	Cos a	Tan b	X (y tan a)	S (y cos a)	Z (S tan b)	Transit Ele. (ft)	Elev (ft)	- Rod to Z (ft)
					Column 7						
1	45°07'15"	2°58'	1.155	.6544	.0518	207.93	275.03	14.25	4307.10	4292.85	---
2	48°51'00"	2°59'	1.144	.6580	.0521	205.97	273.54	14.26	4307.10	4292.85	---
3	48°48'00"	4°16'	1.142	.6586	.0746	205.61	273.27	20.39	4307.10	4286.71	---
4	48°38'30"	4°22'	1.135	.6607	.0763	204.46	272.41	20.80	4307.10	4286.30	---
5	48°29'15"	4°49'	1.129	.6627	.0842	203.36	271.58	22.88	4307.16	4284.28	---
6	48°29'15"	5°07'	1.129	.6627	.0895	203.36	271.58	24.32	4307.16	4280.84	2.0
7	48°18'00"	4°23'	1.135	.6608	.0766	204.49	272.36	20.88	4307.11	4286.23	---
8	48°36'00"	4°50'	1.134	.6623	.0816	204.16	272.18	22.22	4307.11	4284.89	---
9	48°29'00"	5°36'	1.129	.6628	.0980	203.33	271.59	26.63	4307.18	4280.55	---
10	48°19'00"	6°24'	1.123	.6650	.1121	202.14	270.67	30.36	4307.18	4276.82	---
11	48°18'30"	7°09'	1.122	.6651	.1254	202.08	270.62	33.95	4307.38	4268.43	5.0
12	48°16'30"	7°12'	1.121	.6655	.1263	201.85	270.45	34 17	4307.38	4268.21	5.0
13	48°15'00"	7°09'	1.120	.6658	.1254	201.67	270.31	33.91	4307.38	4265.47	8.0
14	48°15'00"	7°01'	1.120	.6658	.1230	201.67	270.31	33 27	4307.38	4264.11	10.0
					Column 8						
1	46°34'45"	2°41'	1.056	.6873	.0468	190.20	261.87	12.54	430..47	4294.93	---
2	46°03'15"	2°48'	1.037	.6936	.0489	186.74	259.37	12.69	4307.47	4294.78	---
3	45°41'15"	3°10'	1.024	.6985	.0554	184.37	257.56	14.29	4307.47	4293.18	---
4	45°30'15"	3°38'	1.017	.7008	.0636	183.19	256.62	16.35	4307.47	4291.12	---
5	45°31'45"	2°50'	1.030	.6963	.0496	185.50	258.47	12.83	4307.47	4294.64	---
6	46°28'15"	2°36'	1.052	.6887	.0451	189.48	261.35	11.79	4307.10	4295.31	---
7	45°33'30"	2°43'	1.031	.6960	.0474	185.69	258.01	12.27	4307.10	4294.83	---
8	44°50'45"	4°26'	.9946	.7090	.0775	179.03	253.87	19.68	4307.10	4287.42	---
9	44°41'00"	5°03'	.9890	.7110	.0883	178.02	253.16	22.3[illegible]	4307.11	4284.74	---
10	44°37'00"	4°39'	.9867	.7118	.0871	177.60	252.87	22.06	4307.11	4285.06	---
11	44°34'00"	5°23'	.9849	.7124	.0942	177.29	252.65	23.81	4307.11	4282.30	1.0
12	44°34'00"	5°01'	.9849	.7124	.0877	177.29	252.65	22.18	4307.25	4284.97	---
13	44°34'45"	5°39'	.9854	.7122	.0989	177.37	252.70	25.00	4307.15	4282.15	---
14	44°21'30"	5°35'	.9778	.7149	.0977	176.01	251.75	24.61	4307.1[illegible]	4280.54	2.0
15	43°54'00"	5°27'	.9623	.7205	.1042	173.21	249.30	26.04	4307.15	4280.11	1.0
16	44°00'00"	6°08'	.9656	.7193	.1074	173.82	250.22	26.89	4307.18	4280.29	---
17	43°58'15"	6°21'	.9647	.7196	.1112	173.64	250.10	27.83	4307.18	4277.35	2.0
18	44°00'00"	6°21'	.9656	.7193	.1112	173.82	250.22	27.85	4307.25	4279.40	---
19	43°49'00"	7°39'	.9595	.7215	.1343	172.71	249.45	33.51	4307.26	4273.74	---
20	44°10'00"	8°00'	.9713	.7173	.1405	174.83	250.9[illegible]	35.47	4307.23	4271.96	---
21	43°56'00"	7°42'	.9634	.7201	.1352	173.41	249.94	3.7[illegible]	4307.23	4268.44	5.0
22	43°57'00"	7°40'	.9640	.7199	.1346	173.52	250.01	33.[illegible]	4307.26	4273.52	---
23	44°02'00"	8°45'	.9668	.7189	.1539	174.02	250.36	38.54	4307.33	4268.79	---
24	43°49'00"	8°51'	.9651	.7195	.1557	173.72	250.15	38.95	4307.33	4268.38	---
25	43°56'00"	8°59'	.9634	.7201	.1580	173.41	249.94	39.51	4307.33	4264.82	3.0
26	43°52'30"	9°05'	.9614	.7208	.1658	173.06	249.70	41.41	4307.35	4262.94	3.0
27	43°56'00"	9°29'	.9631	.7195	.1670	173.72	250.15	41.79	4307.38	4262.59	3.0
28	43°56'00"	9°25'	.9631	.7197	.1658	173.62	250.08	41.48	4307.38	4260.90	5.0

Obs No	Horizontal Angle from CZ (a)	Vertical Angle from Horizontal (b)	Tan a	Cos a	Tan b	X (y tan a)	S (y cos a)	Z (S tan b)	Transit Elev (ft)	Elev (ft)	+ Rod to Z (ft)
29	43°54'00"	9°38'	.9623	.7205	.1697	173.21	249.80	42.40	4307.33	4260.98	4.0
30	43°52'30"	9°27'	.9614	.7208	.1664	173.06	249.70	41.56	4307.38	4258.82	7.0
31	43°59'00"	9°28'	.9651	.7195	.1667	173.72	250.15	41.72	4307.38	4258.67	7.0
32	43°50'30"	9°13'	.9603	.7212	.1637	172.86	249.56	40.87	4307.38	4256.51	10.0
					Column 9						
1	47°59'15"	2°25'	1.110	.6692	.0422	199.82	268.94	11.35	4307.47	4296.12	---
2	46°17'00"	1°37'	1.045	.6910	.0282	188.24	260.45	7.35	4307.47	4300.12	---
3	42°03'12"	2°23'	.9025	.7424	.0416	162.45	242.45	10.09	4307.47	4297.38	---
4	40°58'30"	1°30'	.8685	.7549	.0611	156.33	238.41	14.58	4307.47	4294.89	-2.0
5	39°37'15"	5°33'	.8278	.7702	.0971	149.01	233.68	22.71	4307.11	4284.40	---
6	39°48'00"	4°48'	.8331	.7662	.0839	149.97	234.28	19.67	4307.11	4287.44	---
7	39°20'45"	5°28'	.8198	.7733	.0957	147.56	232.75	22.28	4307.11	4284.83	---
8	38°06'45"	5°34'	.7844	.7868	.1033	141.20	228.77	23.64	4307.11	4283.47	---
9	39°24'45"	7°02'	.8217	.7725	.1233	147.91	232.98	28.74	4307.24	4278.50	---
10	36°48'00"	8°15'	.8040	.7793	.1449	144.84	230.96	33.49	4307.24	4273.75	---
11	37°15'30"	7°30'	.7606	.7969	.1673	136.91	225.87	37.80	4307.18	4269.38	---
12	37°04'30"	10°12'	.7556	.7978	.1799	136.00	225.60	40.59	4307.18	4266.59	---
13	37°12'00"	9°39'	.7990	.7965	.1697	136.62	225.98	38.36	4307.25	4268.89	---
14	37°09'00"	10°10'	.7558	.7977	.1793	136.05	225.63	40.46	4307.25	4266.79	---
15	37°15'30"	10°10'	.7606	.7969	.1793	136.91	225.87	40.91	4307.25	4266.74	---
16	37°04'00"	10°17'	.7553	.7979	.1814	135.96	225.58	40.93	4307.25	4268.32	-2.0
17	37°04'00"	10°26'	.7553	.7979	.1841	135.96	225.58	41.54	4307.25	4267.71	-2.0
18	36°51'00"	10°33'	.7454	.8002	.1862	134.90	224.94	41.89	4307.25	4271.36	-5.0
19	36°55'30"	10°10'	.7508	.7988	.1793	135.51	225.31	40.40	4307.33	4260.93	6.0
20	36°52'00"	11°12'	.7499	.8000	.1980	134.98	224.99	44.55	4307.33	4260.78	2.0
21	36°55'00"	11°19'	.7512	.7995	.2001	135.22	225.13	45.06	4307.33	4261.27	1.0
22	36°48'00"	11°07'	.7480	.8007	.1964	134.65	224.79	44.17	4307.33	4259.16	4.0
23	36°42'00"	11°28'	.7453	.8017	.2119	134.16	224.50	47.58	4307.35	4258.77	1.0
24	36°42'00"	11°48'	.7453	.8017	.2089	134.16	224.50	46.90	4307.35	4256.45	4.0
25	36°48'00"	11°53'	.7480	.8007	.2104	134.65	224.79	47.30	4307.35	4255.05	5.0
26	36°57'30"	12°54'	.7528	.7990	.2107	135.43	224.71	47.33	4307.35	4253.98	6.0
27	36°51'30"	11°57'	.7491	.8018	.2116	134.12	224.47	47.51	4307.35	4253.84	6.0
28	36°37'30"	13°09'	.7413	.8025	.2336	133.80	224.28	52.40	4307.35	4259.95	4.0
29	36°16'00"	13°12'	.7318	.8062	.2345	132.06	223.24	52.37	4307.35	4250.98	4.0
30	36°06'00"	13°15'	.7294	.8079	.2357	131.25	222.77	52.53	4307.35	4245.82	9.0
					Column 13						
1	44°58'45"	1°28'	.9998	.7073	.0256	179.86	254.46	6.52	4307.27	4300.75	---
2	42°31'00"	1°48'	.9174	.7368	.0314	165.13	244.27	7.68	4307.27	4299.57	---
3	39°10'00"	3°30'	.8166	.7753	.0611	146.63	232.16	14.20	4306.97	4292.77	---
4	38°52'30"	5°31'	.8021	.7785	.0877	145.11	231.20	20.30	4306.97	4286.67	---
5	39°39'30"	5°22'	.8207	.7698	.0939	149.21	233.80	21.96	4306.97	4285.01	---

CONFIDENTIAL

Obs No	Horizontal Angle from GZ (a)	Vertical Angle from Horizontal (b)	Tan a	Cos a	Tan b	X (y tan a)	S (y/cos a)	Z (S tan b)	Transit Elev (ft)	Elev (ft)	+ Rod to Z (ft)
6	29°12'30"	4°19'	.6158	.7748	.0754	146.84	232.30	17.53	4306.97	4289.44	---
7	39°32'30"	3°09'	.8255	.7711	.0538	148.60	233.41	12.57	4306.97	4294.40	---
8	38°27'30"	5°32'	.7942	.7720	.0968	142.96	233.13	22.59	4307.23	4284.66	---
9	37°45'00"	7°11'	.7742	.7906	.1260	139.37	227.64	28.69	4307.25	4278.56	---
10	37°26'00"	7°29'	.7654	.7940	.1313	137.78	226.68	29.78	4307.33	4277.55	---
11	37°19'30"	7°33'	.7624	.7735	.1325	137.24	232.68	30.84	4307.35	4276.51	---
12	37°43'00"	8°08'	.7733	.7910	.1429	139.20	227.54	32.52	4307.35	4274.83	---
13	37°18'30"	9°15'	.7620	.7737	.1628	137.16	232.63	37.89	4307.35	4269.46	---
14	36°49'30"	10°08'	.7487	.8004	.1787	134.77	224.86	40.19	4307.35	4276.16	---
15	36°16'30"	10°25'	.7339	.8061	.1838	132.10	223.27	41.05	4307.35	4264.30	2.0
16	36°23'00"	10°22'	.7368	.8050	.1829	132.62	223.58	40.90	4307.38	4266.48	---
17	36°11'00"	11°06'	.7269	.8088	.1961	130 85	222.53	43.66	4307.38	4262.72	1.0
18	36°16'30"	10°52'	.7339	.8061	.1919	132.10	223.27	42.86	4307.38	4260.52	4.0
19	35°58'00"	11°09'	.7256	.8093	.1970	130.61	222.39	43.83	4307.38	4257.55	6.0
20	38°38'00"	7°34'	.7992	.78115	.0975	143.5	230.5	22.45	4307.25	4284.80	---
21	35°26'00"	11°48'	.7115	.81479	.2089	128.1	220.9	46.15	4307.44	4252.29	0.9
22	35°21'00"	11°58'	.7094	.8156	.2020	127.7	220.7	46.79	4307.44	4250.36	10.0
23	35°10'00"	12°04'	.7046	.8175	.2138	126.8	220.2	47.08	4307.44	4250.36	10.0
24	35°19'00"	12°[illegible]	.7085	.8150	.2132	127.5	220.6	47.03	4307.44	4249.41	11.0
25	34°33'00"	12°31'	.6886	.8236	.2220	124.0	218.5	48.51	4307.44	4245.93	13.0
					Column 14						
1	46°[illegible]'00"	1°15'	1.069	.6830	.0219	192.46	263.51	5.79	4307.27	4296.48	5.0
2	45°44'30"	4°12'	1.026	.6978	.0734	184.72	257.91	18.9[illegible]	4307.25	4288.31	---
3	45°37'30"	4°0.0'	1.022	.6993	.0728	183.96	257.38	18.7[illegible]	4307.25	4290.50	-2.0
4	45°32'00"	4°34'	1.018	.7004	.0798	183.38	256.96	20.5[illegible]	4307.33	4286.81	---
5	45°28'00"	4°51'	1.016	.7013	.0854	182.95	256.65	21.9[illegible]	4307.33	4285.40	---
6	45°28'00"	4°46'	1.016	.7013	.0833	182.95	256.65	21.46	4307.33	4283.93	2.0
7	45°22'30"	4°49'	1.013	.7024	.0842	182.37	256.24	21.59	4307.33	4280.74	5.0
8	45°20'00"	3°44'	1.011	.7029	.0652	182.10	256.05	16.71	4307.35	4280.64	10.0
9	45°02'00"	6°12'	1.001	.7066	.1086	180.20	254.70	27.67	4307.35	4279.68	---
10	45°02'00"	6°12'	1.001	.7066	.1086	180.20	254.70	27.67	4307.35	4274.68	5.0
11	45°00'00"	6°26'	1.000	.7071	.1127	180.00	254.55	28.70	4307.35	4273.65	5.0
12	44°52'00"	8°08'	.9953	.7087	.1429	179.16	253.96	36.30	4307.38	4268.08	3.0
13	44°46'00"	8°03'	.9776	.7079	.1414	179.58	254.2[illegible]	[illegible].[illegible]	4307.38	4264.42	7.0
14	46°10'00"	2°28'	.[illegible]	.6926	.0431	188.0	260.0	11.[illegible]	4307.25	4296.05	---
15	46°01'30"	3°24'	[illegible]	.6930	.0594	186.5	260.0	15.45	4307.25	4291.80	---
16	45°59'00"	3°24'	1.0[illegible]	.6969	.0594	185.0	258.0	15.30	4307.25	4291.95	---
17	45°42'00"	3°22'	1.020	.7004	.0676	183.5	257.0	17.40	4307.25	4289.85	---
18	45°47'30"	4°[illegible]'	1.023	.6992	.0720	184.3	257.5	18.55	4307.33	4288.78	---
19	44°52'00"	3°39'	.9954	.7089	.1521	179.2	253.9	38.62	4307.44	4264.82	4.0
20	44°32'00"	9°07'	.9938	.7128	.1605	177.1	252.5	40.53	4307.44	4263.91	3.0
21	44°25'00"	9°13'	.9799	.7143	.1623	176.4	251.9	40.88	4307.44	4258.56	8.0

Obs No	Horizontal Angle from GZ (a)	Vertical Angle from Horizontal (b)	Tan a	Cos a	Tan b	X (y tan a)	S (y/cos a)	Z (S tan b)	Transit Elev (ft)	Elev (ft)	+ Rod to Z (ft)
					Column 15						
1	48°54'30"	3°08'	1.146	.6572	.0547	206.39	273.86	14.99	4307.25	4292.26	---
2	48°52'30"	2°55'	1.145	.6577	.0509	206.15	273.67	13.94	4307.25	4268.31	5.0
3	48°46'00"	4°12'	1.140	.6591	.0734	205.37	273.08	20.05	4307.33	4286.28	1.0
4	48°35'00"	4°03'	1.133	.6615	.0708	204.05	272.09	19.27	4307.33	4286.06	2.0
5	48°34'00"	4°05'	1.132	.6617	.0713	203.93	272.00	19.42	4307.33	4282.91	5.0
6	48°31'30"	4°04'	1.131	.6622	.0710	203.63	271.78	19.32	4307.33	4281.01	7.0
7	48°24'00"	5°10'	1.126	.6639	.0904	202.73	271.11	24.51	4307.35	4278.84	4.0
8	48°19'30"	5°18'	1.123	.6649	.0927	202.20	270.71	25.11	4307.35	4278.24	4.0
9	48°18'00"	5°22'	1.122	.6652	.0939	202.02	270.58	25.42	4307.35	4275.93	6.0
10	48°00'00"	2°35'	1.150	.6561	.0449	207.0	274.0	12.30	4307.11	4292.81	2.0
11	48°12'00"	6°51'	1.118	.667	.1201	201.2	270.2	32.43	4307.44	4274.61	1.0
12	48°15'00"	6°56'	1.121	.666	.1215	201.8	270.3	32.84	4307.44	4273.6	1.0
13	48°14'00"	6°49'	1.120	.666	.1195	200.7	270.2	31.99	4307.44	4270.45	5.0
14	48°12'	6°45'	1.118	.667	.1184	201.2	270.0	31.97	4307.44	4267.47	8.0
					Column 16						
1	51°32'00"	2°32'	1.273	.6174	.0500	229.28	291.50	14.30	4307.33	4290.73	2.0
2	51°30'30"	2°33'	1.272	.6178	.0503	229.09	291.33	14.67	4307.33	4290.66	2.0
3	51°28'30"	2°39'	1.271	.6182	.0521	228.80	291.12	15.17	4307.33	4290.16	2.0
4	51°27'30"	2°37'	1.270	.6185	.0515	228.67	291.01	15.00	4307.33	4286.33	6.0
5	51°27'00"	2°33'	1.270	.6186	.0576	228.60	290.96	16.73	4307.33	4284.55	6.0
6	51°24'00"	2°33'	1.267	.6193	.0570	228.19	290.64	16.59	4307.33	4283.74	7.0
7	51°13'30"	2°48'	1.259	.6217	.0652	226.76	289.52	18.97	4307.35	4283.38	5.0
8	51°33'30"	2°43'	1.259	.6217	.0649	226.76	289.52	18.82	4307.35	4283.54	5.0
9	51°35'30"	2°46'	1.261	.6212	.0658	227.03	289.73	19.07	4307.35	4280.28	8.0
10	51°27'00"	5°24'	1.255	.6232	.0946	225.9	288.8	27.32	4307.44	4273.12	7.0
					Column 17						
1	54°28'30"	2°51'	1.400	.5810	.0497	252.11	309.77	15.47	4307.33	4291.91	---
2	54°28'30"	2°49'	1.400	.5810	.0492	252.11	309.77	15.24	4307.33	4287.09	5.0
3	54°27'00"	2°30'	1.399	.5814	.0436	251.88	309.50	13.58	4307.33	4285.81	8.0
4	54°21'00"	2°29'	1.394	.5828	.0433	250.93	308.8	13.42	4307.33	4283.94	10.0
5	54°23'00"	3°02'	1.395	.5823	.0529	251.26	309.08	16.51	4307.35	4283.97	7.0
6	54°17'00"	3°45'	1.384	.5838	.0656	248.6	308.3	20.22	4307.44	4280.22	7.0
					Column 18						
1	56°48'00"	2°47'	1.528	.5764	.0486	275.07	312.26	15.18	4307.33	4292.15	---
2	56°54'30"	2°57'	1.534	.5759	.0492	276.20	329.68	16.22	4307.33	4287.11	4.0
3	56°58'00"	2°49'	1.537	.5740	.0492	276.82	313.55	15.43	4307.33	4285.90	6.0
					Column 19						
1	59°09'00"	2°49'	1.674	.5127	.0492	301.35	351.01	17.27	4307.33	4287.06	3.0
2	59°03'00"	2°50'	1.667	.5142	.0494	300.16	349.99	17.32	4307.33	4290.01	---

Obs No	Horizontal Angle from CZ (a)	Vertical Angle from Horizontal (b)	Tan a	Cos a	Tan b	X (y tan a)	S (y cos a)	Z (S tan b)	Transit Elev (ft)	Elev (ft)	+ Rod to Z (ft)
					Column 20						
1	61°04'30"	1°34'	1.809	.4836	.0273	325.73	372.15	10.18	4307.33	4291.15	6.0
2	61°08'30"	2°24'	1.814	.4826	.0419	326.63	372.94	15.63	4307.33	4288.70	3.0
3	61°08'30"	2°27'	1.814	.4826	.0427	326.63	372.94	15.96	4307.33	4288.37	3.0
					Column 21						
1	62°45'00"	2°47'	1.941	.4578	.0398	349.49	393.12	15.67	4307.33	4291.66	---
2	62°50'00"	2°24'	1.948	.4565	.0389	350.74	394.23	15.37	4307.33	4268.96	3.0
					Column 11						
1	0°00'00"	29°30'	0.000	0.000	0.5735	0.000	(.5735X180 = 103.23'	59.20	4307.33	4204.10 - 44.10 4159.00	42.0

CONFIDENTIAL

REFERENCES

1. Physical Characteristics of Crater and Lip; Project 4.2, Operation JANGLE, WT-339; CONFIDENTIAL

2. Perkins, B. Jr.; A New Technique for Studying Crater Phenomena; BRL Tech Note 880, March 1954.

3. Small Explosion Tests; Phase II-B of Project MOLE, AFSWP-290, SRI, December 1951; SECRET.

4. Study of Energy Partitioning for Partially Confined Explosives; AFSWP-788, Waterways Experiment Station, November 1[illegible]; CONFIDENTIAL.

5. Effects of Stemming on Underground Explosions; AFSWP-223, Waterways Experiment Station, March 1956, Preliminary Report; CONFIDENTIAL.

6. Swift, L. M. and Sachs, D. C.; Underground Explosion Effects; Project 1.7, Operation TEAPOT, ITR-1106, May 1955; SECRET RESTRICTED DATA.

7. Porzel, F. B.; Theoretical Aspects of Nuclear Blast Hydrodynamics; LAMS-1868, LASL, December 1954; SECRET RESTRICTED DATA.

8. Small Explosion Tests; Final Report Project MOLE, AFSWP-291, Volume I, SRI, December 1955; SECRET RESTRICTED DATA.

9. Anderson, F. W.; Crater Dimensions from Experimental Data, FWE-18, Ministry of Home Security, Research and Experiments Department, September 1942; Addendum September 1953; CONFIDENTIAL.

10. Effects of Impact and Explosion; Volume I, Division 2. NDRC, OSRD, 1946; CONFIDENTIAL.

11. Christensen, W. J.; LCDR, CEC, USN; Cratering from Atomic Weapons; AFSWP 514, 29 June 1956; SECRET RESTRICTED DATA.

DISTRIBUTION

Military Distribution Category 3-32

ARMY ACTIVITIES

1 Asst. Dep. Chief of Staff for Military Operations, D/A, Washington 25, D.C. ATTN: Asst. Executive (R&M)
2 Chief of Research and Development, D/A, Washington 25, D.C. ATTN: Atomic Division
3 Chief of Ordnance, D/A, Washington 25, D.C. ATTN: ORDTX-AR
4 Chief Signal Officer, D/A, R&D Division, Washington 25, D.C. ATTN: SIGRD-8
5 The Surgeon General, D/A, Washington 25, D.C. ATTN: MEDNC
6-7 Chief Chemical Officer, D/A, Washington 25, D.C.
8 The Quartermaster General, D/A, Washington 25, D.C. ATTN: Research and Development
9-11 Chief of Engineers, D/A, Washington 25, D.C. ATTN: ENGEB
12 Chief of Transportation, Military Planning and Intelligence Div., Washington 25, D.C.
13-17 Commanding General, Headquarters, U. S. Continental Army Command, Ft. Monroe, Va.
18 President, Board #1, Headquarters, Continental Army Command, Ft. Sill, Okla.
19 President, Board #2, Headquarters, Continental Army Command, Ft. Knox, Ky.
20 President, Board #4, Headquarters, Continental Army Command, Ft. Bliss
21 Commanding General, U.S. [illegible] Caribbean, Ft. Amador, C.Z. ATTN: Cml. Off.
22-23 Commanding General, U.S. [illegible] Europe, APO 403, New York, N.Y. ATTN: OPOT [illegible] Combat Dev. Br.
24-25 Commandant, Command and [illegible] Staff College, Ft. Leavenworth, Kan. ATTN: [illegible](AS)
26 Commandant, The Artil[illegible] and Missile School, Ft. Sill, Okla.
27 Secretary, The U.S. Army Air Defense School, Ft. Bliss, Texas. ATTN: Mr. Bryce V. Reth, Dept. of Tactics and Combat Arms
28 Commanding General, Army Medical Service School, Brooke Army Medical Center, Ft. Sam Houston, Tex.
29 Director, Special Weapons Development Office, Headquarters, CONARC, Ft. Bliss, Tex. ATTN: Capt. T. E. Salmon
30 Commandant, Walter Reed Army Institute of Research, Walter Reed Army Medical Center, Washington 25, D. C.
31 Superintendent, U.S. Military Academy, West Point, N. Y. ATTN: Prof. of Ordnance
32 Commandant, Chemical Corps School, Chemical Corps Training Command, Ft. Mac[illegible], Ala.
33 Commanding General, U.S. Army Chemical Corps, Research and Development Command, Washington, D.C.
34-35 Commanding General, Aberdeen Proving Grounds, Md. ATTN: Director, Ballistics Research Laboratory
36 Commanding General, The Engineer Center, Ft. Belvoir, Va. ATTN: Asst. Commandant, Engineer School
37 Commanding Officer, Engineer Research and Development Laboratory, Ft. Belvoir, Va. ATTN: Chief, Technical Intelligence Branch
38 Commanding Officer, Picatinny Arsenal, Dover, N.J. ATTN: [illegible]
39 Commanding Officer, Army Medical Research Laboratory, Ft. Knox, Ky.
40-41 Commanding Officer, Chemical Warfare Laboratories, Army Chemical Center, Md. ATTN: Tech. Library
42 Commanding Officer, Transportation Aid Station, Ft. Eustis, Va.
43 Director, Technical Intelligence Center, Signal Intelligence Service, Arlington, D.C.
44 Director, Waterways Experiment Station, P.O. Box 631, Vicksburg, Miss. ATTN: Library
45 Director, Armed Forces Institute of Pathology, Walter Reed Army Medical Center, 6825 16th Street, N.W., Washington 12, D.C.
46 Operations Research Office, Johns Hopkins University, 6935 Arlington Rd., Bethesda 14, Md.
47-48 Commanding General, Quartermaster Research and Development Command, Quartermaster Research and Development Center, Natick, Mass. ATTN: CBR Liaison Officer
47 Commandant, U.S. Army Aviation School, Fort Rucker, Ala.
48 Commanding [illegible], Diamond Ordnance Fuze Laboratories, Washington 25, D.C., ATTN: Coordinator, Atomic Weapons Effects Tests
49 Commanding General, Quartermaster Research and Engineering Command U.S. Army, Natick, Mass.
50-54 Technical Information Service Extension, Oak Ridge, Tenn.

NAVY ACTIVITIES

55-56 Chief of Naval Operations, D/N, Washington 25, D. C. ATTN: OP-36
57 Chief of Naval Operations, D/N, Washington 25, D.C. ATTN: OP-03EG
58 Chief, Bureau of Medicine and Surgery, D/N, Washington 25, D.C. ATTN: Special Weapons Defense Div.
59 Chief, Bureau of Ordnance, D/N, Washington 25, D.C.
60 Chief, Bureau of Ships, D/N, Washington 25, D.C. ATTN: Code 348
61 Chief, Bureau of Yards and Docks, D/N, Washington 25, D.C. ATTN: D-440
62 Chief, Bureau of Supplies and Accounts, D/N, Washington 25, D.C.
63-64 Chief, Bureau of Aeronautics, D/N, Washington 25, D.C.
65 Chief of Naval Research, Department of the Navy Washington 25, D.C. ATTN: Code 811
66 Commander-in-Chief, U.S. Atlantic Fleet, U.S. Naval Base, Norfolk [illegible], Va.
67-70 Commandant, U.S. Marine Corps, Washington 25, D.C. ATTN: Code [illegible]
71 President, U.S. Naval War College, Newport, R.I.
72 Superintendent, U.S. Naval Postgraduate School, Monterey, Calif.
73 Commanding Officer, U.S. Naval Schools Command, U.S. Naval Station, Treasure Island, San Francisco, Calif.
74 Commanding Officer, U.S. Fleet Training Center, Naval Base, Norfolk 11, Va. ATTN: Special Weapons School
75-76 Special Weapons Unit, Pacific, U.S. Naval Air Station, North Island, San Diego 35, Calif.
77 Commanding Officer, U.S. Naval Damage Control Training Center, Naval Base, Philadelphia, Pa. ATTN: ABC Defense Course
78 Commander, U.S. Naval Ordnance Laboratory, Silver Spring 19, Md. ATTN: [illegible]
79 Commander, U.S. Naval Ordnance Laboratory, Silver Spring 19, Md. ATTN: R
80 Commander, U.S. Naval Ordnance Test Station, Inyokern, China Lake, Calif.
81 Officer-in-Charge, U.S. Naval Civil Engineering Res. and Evaluation Lab., U.S. Naval Construction Bn. Center, Port Hueneme, Calif. ATTN: Code 753
82 Commanding Officer, U.S. Naval Medical Research Inst., National Naval Medical Center, Bethesda 14, Md.
83 Director, Naval Air Experimental Station, Air Material Center, U.S. Naval Base, Philadelphia, Penn.

84 Director, U.S. Naval Research Laboratory, Washington 25, D.C. ATTN: Mrs. Katherine H. Cass
85 Commanding Officer and Director, U.S. Navy Electronics Laboratory, San Diego 52, Calif. ATTN: Code 4223
86- 87 Commanding Officer, U.S. Naval Radiological Defense Laboratory, San Francisco, Calif. ATTN: Technical Information Division
88- 89 Commanding Officer and Director, David W. Taylor Model Basin, Washington 7, D.C. ATTN: Library
90 Commander, U.S. Naval Air Development Center, Johnsville, Pa.
91 Commanding Officer and Director, U.S. Naval Engineering Experiment Station, Annapolis, Md. ATTN: Code 155
92 Commander-in-Chief Pacific, Pearl Harbor, TH
93 Commander, Norfolk Naval Shipyard, Portsmouth 8, Va. ATTN: Code 270
94- 98 Technical Information Service Extension, Oak Ridge, Tenn (Surplus)

AIR FORCE ACTIVITIES

99 Asst. for Atomic Energy Headquarters, USAF, Washington 25, D.C. ATTN: DCS/O
100 Director of Operations, Headquarters, USAF, Washington 25, D.C. ATTN: Operations Analysis
101 Director of Plans, Headquarters, USAF, Washington 25, D.C. ATTN: War Plans Div.
102 Director of Research and Development, DCS/D, Headquarters, USAF, Washington 25, D.C. ATTN: Combat Components Div.
103-104 Director of Intelligence, Headquarters, USAF, Washington 25, D.C. ATTN: AFOIN-IB2
105 The Surgeon General, Headquarters, USAF, Washington 25, D.C. ATTN: Bio. Def. Br., Pre. Med. Div.
106 Asst. Chief of Staff, Intelligence, Headquarters, U.S. Air Forces-Europe, APO 633, New York, N.Y. ATTN: Directorate of Air Targets
107 Commander, 497th Reconnaissance Technical Squadron (Augmented), APO 633, New York, N.Y.
108 Commander-in-Chief, Pacific Air Forces, APO 953, San Francisco, Calif. ATTN: PFOIK-MB, Base Recovery
109 Commander-in-Chief, Strategic Air Command, Offutt AFB, Omaha, Nebraska. ATTN: OAWS
110 Commander, Tactical Air Command, Langley AFB, Va. ATTN: Documents Security Branch
111 Commander, Air Defense Command, Ent AFB, Colo.
112-113 Research Directorate, Headquarters, Air Force Special Weapons Center, Kirtland AFB, New Mexico. ATTN: Blast Effects Res.
114-116 Assistant for Operations Analysis, DCS/Operations, ATTN: Missile Survival Study Group (Mr. Tuttle), Headquarters, USAF, Washington 25, D.C.
117 Director of Installations, DCS/O, Headquarters, USAF, Washington 25, D.C. ATTN: AFOIE-2
118 Commander, Air Research and Development Command, Andrews AFB, Washington 25, D.C. ATTN: RDDN
119 Commander, Air Proving Ground Command, Eglin AFB, Fla. ATTN: Adj./Tech. Report Branch
120-121 Director, Air University Library, Maxwell AFB, Ala.
122-127 Commander, Air Training Command, Randolph AFB, Tex.
128-129 Commandant, Air Force School of Aviation Medicine, Randolph AFB, Tex.
130-135 Commander, Wright Air Development Center, Wright-Patterson AFB, Dayton, Ohio. ATTN: WCOSI
136-137 Commander, Air Force Cambridge Research Center, LG Hanscom Field, Bedford, Mass. ATTN: CRQST-2
138-140 Commander, Air Force Special Weapons Command, Kirtland AFB, N. Mex. ATTN: Tech. Infor. Office
141 Commander, Lowry AFB, Denver, Colo. ATTN: Department of Special Weapons Training
142 Commander, 1009th Special Weapons Squadron, Headquarters, USAF, Washington 25, D.C.
143-144 The RAND Corporation, 1700 Main Street, Santa Monica, Calif. ATTN: Nuclear Energy Division
145 Commander, Second Air Force, Barksdale AFB, La. ATTN: Operations Analysis Office
146 Commander, Eighth Air Force, Westover AFB, Mass. ATTN: Operations Analysis Office
147 Commander, Fifteenth Air Force, March AFB, Calif. ATTN: Operations Analysis Office
148 Commander, Western Development Div. (ARDC), PO Box 262, Inglewood, Calif. ATTN: Major A. G. Keitz
149-153 Technical Information Service Extension, Oak Ridge, Tenn. (Surplus)

OTHER DEPARTMENT OF DEFENSE ACTIVITIES

154 Asst. Secretary of Defense, Research and Engineering, D/D, Washington 25, D.C. ATTN: Tech. Library
155 U.S. Documents Officer, Office of the U.S. National Military Representative, SHAPE, APO 55, New York, N.Y.
156 Director, Weapons Systems Evaluation Group, OSD, Rm 2E1006, Pentagon, Washington 25, D.C.
157 Chairman, Armed Services Explosives Safety Board, D/D, Building T-7, Gravelly Point, Washington 25, D.C.
158 Commandant, Armed Forces Staff College, Norfolk 11, Va. ATTN: Secretary
159 Commander, Field Command, Armed Forces Special Weapons Project, PO Box 5100, Albuquerque, N. Mex.
160 Commander, Field Command, Armed Forces Special Weapons Project, PO Box 5100, Albuquerque, N. Mex. ATTN: Technical Training Group
161-165 Commander, Field Command, Armed Forces Special Weapons Project, P.O. Box 5100, Albuquerque, N. Mex. ATTN: Deputy Chief of Staff, Weapons Effects Test
166-176 Chief, Armed Forces Special Weapons Project, Washington 25, D.C. ATTN: Documents Library Branch
177 Technical Information Service Extension, Oak Ridge, Tenn. (Surplus)

ATOMIC ENERGY COMMISSION ACTIVITIES

178-180 U.S. Atomic Energy Commission, Classified Technical Library, Washington 25, D.C. ATTN: Mrs. J. M. O'Leary (For DMA)
181-182 Los Alamos Scientific Laboratory, Report Library, PO Box 1663, Los Alamos, N. Mex. ATTN: Helen Redman
183-187 Sandia Corporation, Classified Document Division, Sandia Base, Albuquerque, N. Mex. ATTN: W. J. Smyth, Jr.
188-190 University of California Radiation Laboratory, PO Box 808, Livermore, Calif. ATTN: Clovis G. Craig
191 Weapon Data Section, Technical Information Service Extension, Oak Ridge, Tenn.
192-200 Technical Information Service Extension, Oak Ridge, Tenn. (Surplus)